Magma evolution at La Fossa volcano (Vulcano Island, Italy) in the last 1000 years: evidence from eruptive products and temperature gradient experiments

Simone Costa, M. Masotta, A. Gioncada, M. Pistolesi, Delphine Bosch, P. Scarlato

Magma evolution at La Fossa volcano (Vulcano Island, Italy) in the last 1000 years: evidence from eruptive products and temperature gradient experiments

S. Costa[1,2] · M. Masotta[2] · A. Gioncada[2] · M. Pistolesi[2] · D. Bosch[3] · P. Scarlato[4]

Abstract
The intense explosive and effusive volcanic activity of the last 1000 years at La Fossa volcano (Vulcano Island, Italy) was characterized by the eruption of magmas ranging in composition from latites to trachytes and rhyolites, as well as K-rich trachytes. Evidence of syn-eruptive mixing among these magmas is frequently observed in the form of magmatic enclaves and bands in lava flows and pyroclastic products. The petrological and volcanological diversity of the erupted materials suggests that complex differentiation processes occurred in the shallow part of the plumbing system. With the aim to reconstruct the magmatic feeding system and to identify the differentiation processes behind such a petrologic complexity, we analysed lavas and pyroclastic products representative of the recent eruptive sequences at La Fossa and combined the petro-chemical features with thermo-barometric calculations, geochemical modelling and temperature gradient experiments. Thermo-barometric calculations indicate that the K-rich trachytic magma crystallized at lower pressure (160 ± 54 MPa) compared to the latitic (307 ± 47 MPa) and trachytic (208 ± 30 MPa) magmas. Differentiation modelling suggests that both trachytic and rhyolitic compositions can be obtained through differentiation of a common latitic magma, essentially by varying the plagioclase/sanidine ratio. Temperature gradient experiments, performed at the conditions inferred for the shallow plumbing system of La Fossa volcano (150 MPa and 1050–900 °C), indicate different paths of melt differentiation that overall produce an increase of the SiO_2/K_2O ratio with the increasing H_2O in the system (from 0 to 4 wt.%). This is consistent with the origin of K-rich trachytes at lower pressure and lower H_2O content. In turn, the formation of crystal-poor rhyolites is explained by the segregation of the interstitial melt formed in a latitic–trachytic crystal mush, favoured by the second boiling of the melt and consequent exsolution of a fluid phase.

Keywords Vulcano Island · Trachyte · Crystal-poor rhyolite · Crystal mush · Temperature gradient experiments

Introduction

The physico-chemical characterization of the plumbing system of frequently active arc volcanoes is one of the main challenges in volcanology, as it constitutes a ground element for the assessment of the pre-eruptive conditions of magmas and for the definition of future eruptive scenarios. On the one hand, the estimate of the intensive variables of the magma is possible either through the thermo-barometric calculations based on the phase compositions of eruptive products (Putirka 2008), or via direct comparison of the natural products with laboratory experiments performed under constrained physical conditions (Scaillet et al. 2008). On the other hand, clues on the chemical composition of magmas feeding the eruptions can be obtained through the petrologic study of the eruptive products of the

✉ S. Costa
simone.costa@unifi.it

1 Dipartimento Di Scienze Della Terra, Università Di Firenze, via La Pira, 4 50121 Florence, Italy

2 Dipartimento Di Scienze Della Terra, Università Di Pisa, via S. Maria, 53 56126 Pisa, Italy

3 Géosciences Montpellier, Université de Montpellier, Place E. Bataillon, 34095 Montpellier, France

4 Istituto Nazionale Di Geofisica E Vulcanologia, Via di Vigna Murata 605, 00191 Rome, Italy

recent volcanic activity (Cioni et al. 1998). Such information, combined with data obtained from the geochemical and geophysical monitoring, is critical for determining the variations of the physico-chemical parameters of magmas and, ultimately, for the volcanic hazard assessment and for designing risk mitigation plans (Neri et al. 2008). In this context, the active volcanic system of La Fossa (Vulcano Island, Italy), with its recurrent historic activity and well-known stratigraphy (De Astis et al. 2013), represents an ideal study case for the investigation of magmatic processes and eruptive dynamics.

The eruptive products of La Fossa encompass a broad range of magma compositions, ranging from latite to trachyte and rhyolite. The heterogeneous composition of magmas erupted even within single eruptions, testifies to syn-eruptive mixing and or mingling processes (De Astis et al. 2013). Latitic to trachytic magmatic enclaves in rhyolitic lavas and compositionally heterogeneous (banded) pumices are, in fact, common in the recent activity of La Fossa volcano (e.g. Piochi et al. 2009; Rossi et al. 2019). Significant variations of magma chemistry at a same SiO_2 content are also observed, as in the case of the fallout products emplaced during the Palizzi–Commenda eruptive cluster (Di Traglia et al. 2013), whose trachytic composition has the highest concentration in K_2O of the entire eruptive history of La Fossa volcano (up to 7.5 wt.%; Fulignati et al. 2018).

The petrological complexity of the plumbing system of La Fossa has been the object of many studies in the past 2 decades, aimed at defining (i) the intensive variables and the magmatic processes governing the evolution of parental magmas (Clocchiatti et al. 1994; De Astis et al. 1997; Del Moro et al. 1998; Gioncada et al. 1998; Pinarelli et al. 2019); (ii) the pre- and syn-eruptive interaction of magmas at different degrees of evolution (Piochi et al. 2009; Bullock et al. 2019); (iii) the dynamics and timescales of pre-eruptive magma ascent, mixing and eruption (Vetere et al. 2015; Nicotra et al. 2018; Rossi et al. 2019). Although there is a general consensus for the pre-eruptive temperature estimates and mixing processes of the latitic, trachytic and rhyolitic magmas erupted at La Fossa (Clocchiatti et al. 1994; Vetere et al. 2015), uncertainty in the determination of pressure of magma storage and volatile content and in the overall relationships among these magmas still exists. This gap of knowledge is in part explained by the fact that most of petrologic studies are focused on lava flows and on the youngest explosive products, which are more easily accessible and better constrained from a chrono-stratigraphic point of view. This inevitably leads to underestimating the significance of the pyroclastic component (e.g. fallout deposits) that constitute the largest fraction of the volume of erupted magmas (Di Traglia et al. 2013). Through the analysis of the pyroclastic products and their distribution in the eruptive sequence, it is thus possible to obtain a broader picture of the plumbing system and to place constraints on magma dynamics and evolution in small arc volcanoes.

In this study, we took in exam the last 1000 years activity of La Fossa volcano, with the aim of reconstructing the physical conditions at which magmas evolved, interacted and erupted. For this purpose, we selected representative rock samples encompassing the entire compositional range of erupted magmas, and combined new whole rock and micro-chemical analyses of natural samples with temperature gradient experiments that emulate the crystallization and differentiation processes occurring in a shallow and temperature-zoned magma reservoir. The results obtained in this work contribute to envisage the complexity of the polybaric storage system of La Fossa volcano, where the role of shallow crystal mushes is determinant for the production of small volumes of rhyolitic magmas at rather short timescale, through repeated episodes of melt extraction.

Geological background and stratigraphy of the last 1000 years of La Fossa

Vulcano is the southernmost island of the Aeolian archipelago, a volcanic arc located in southern Tyrrhenian sea (Fig. 1). La Fossa cone, located in the northern sector of the island and active since 6 ka, last erupted in AD 1888–1890 (Keller 1980). The stratigraphy of La Fossa cone has been described in detail in many studies and consists mainly of pyroclastic fallout deposits (ash, pumiceous lapilli, blocks and bread crust bombs) and lava flows (Clocchiatti et al. 1994; Piochi et al. 2009; Di Traglia et al. 2013; De Astis et al. 2013). Following the stratigraphic reconstruction proposed by Di Traglia et al. (2013), the eruptive history of the last 1000 years can be summarized in two eruptive clusters: the Palizzi–Commenda eruptive cluster (PCEC), developed during the thirteenth century, and the Gran Cratere eruptive cluster (GCEC, fifteenth century-1890 AD) (Fig. 2a). The stratigraphic sequence of PCEC displays a large variety of eruptive products and a wide spectrum of magma compositions, ranging from latite to trachyte and rhyolite (Fig. 2b): (i) latitic and trachytic cross-stratified and parallel-bedded ash layers (Pal A and Pal C); (ii) pumiceous fallout layers of rhyolitic and trachytic composition (Pal B and Pal D, respectively); (iii) lava flows, including the rhyolitic obsidian Commenda lava and the trachytic lava flows of Palizzi, Campo Sportivo and Punte Nere; (iv) ash layers and widely dispersed pyroclastic density currents deposits associated with the hydrothermal eruption of Breccia di Commenda (Gurioli et al. 2012; Rosi et al. 2018). The GCEC includes the products of the Pietre Cotte eruptive unit, consisting of (i) latitic ash and lapilli layers; (ii) rhyolitic pumiceous fallout layers; (iii) the rhyolitic AD 1739 Pietre Cotte lava flow (Piochi et al. 2009; Vetere et al. 2015). The uppermost

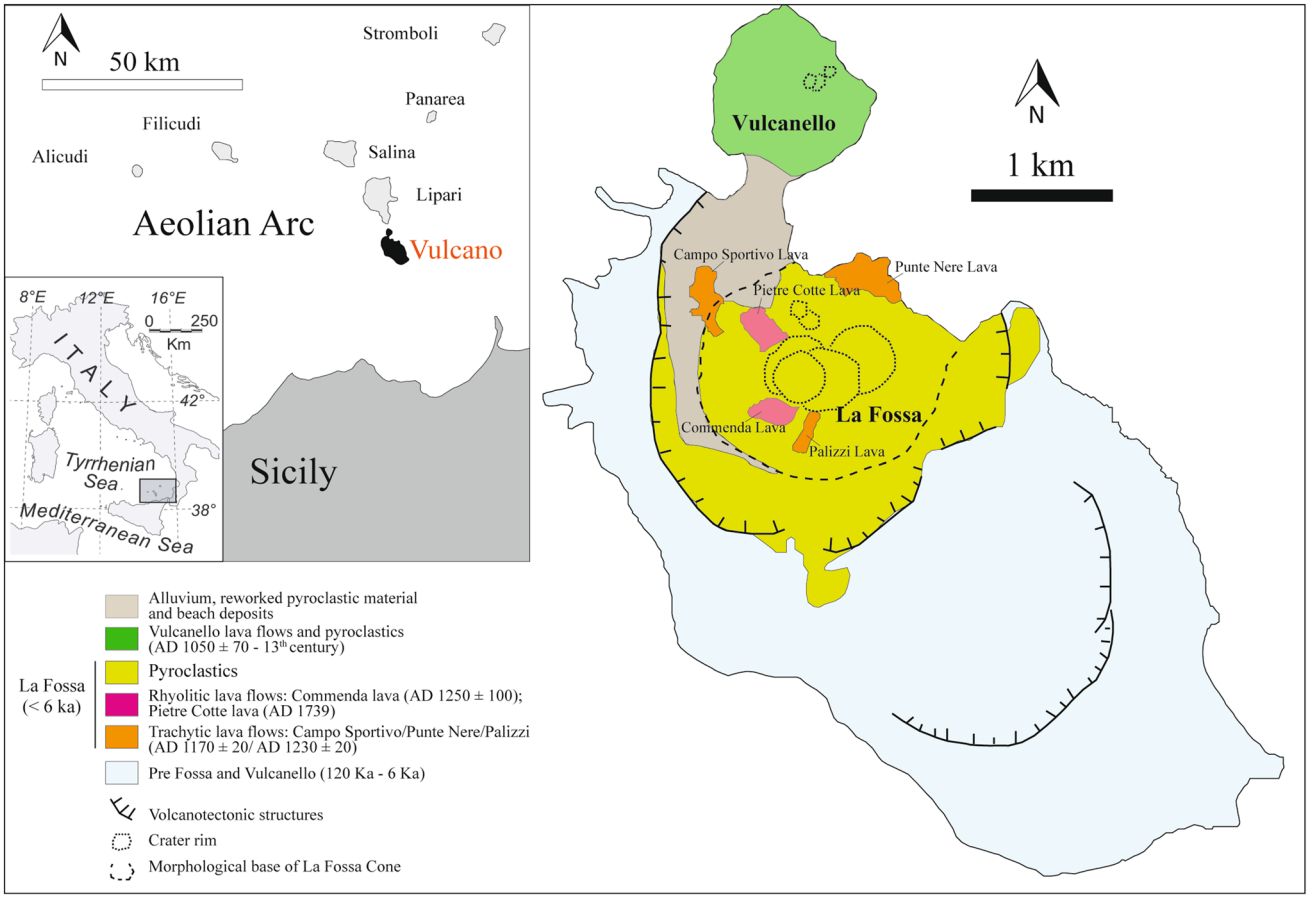

Fig. 1 Sketch map of the Aeolian archipelago and simplified geological map of Vulcano Island (modified after De Astis et al. 2013)

part of the GCEC is represented by the products of the AD 1888–1890 eruption, consisting of latitic spatters, trachytic and rhyolitic ash and lapilli layers and the characteristic bread crust bombs, trachytic and rhyolitic in composition (Clocchiatti et al. 1994).

La Fossa plumbing system

The plumbing system of La Fossa cone has been the object of several studies that reported petrological evidences of magma mixing processes, such as the occurrence of magmatic enclaves and banding of latitic and trachytic compositions within rhyolitic lava flows and pyroclastic products (Frazzetta et al. 1983; De Fino et al. 1991; Clocchiatti et al. 1994; Piochi et al. 2009; De Astis et al. 2013; Bullock et al. 2019; Rossi et al. 2019). The combination of petrological and geochemical data, including melt, fluid inclusions and gas geochemistry (Clocchiatti et al. 1994; Gioncada et al. 1998; Zanon et al. 2003; Paonita et al. 2013; Mandarano et al. 2016), contributed to envisage the plumbing system of La Fossa as a complex polybaric system, represented by multiple reservoirs that have been variably involved during the activity of both La Fossa and Vulcanello (Peccerillo et al. 2006; Davì et al. 2009; De Astis et al. 2013; Fusillo et al. 2015; Nicotra et al. 2018). The deepest reservoir (basaltic to shoshonitic) is presumably located between 21 and 18 km, whereas a shoshonitic to latitic storage level has been hypothesized between ~ 17 and 12 km (De Astis et al. 2013; Nicotra et al. 2018). The shallow crustal reservoirs hosting latitic to trachytic and rhyolitic magmas are presumably located at depths comprised between 5 and 2 km. Based on a recent calibration of a plagioclase–liquid hygrometer, Masotta and Mollo (2019) estimated H_2O contents ranging from 2.5 to 3.5 wt.% for the latitic and trachytic magmas, respectively. An uppermost rhyolitic reservoir located at depth of about 1–2 km has been suggested by Clocchiatti et al. (1994) and Zanon et al. (2003). These authors studied secondary fluid inclusions contained in metamorphic xenoliths, yielding to equilibration pressure and temperature of 30–60 MPa and ~ 1000 °C, respectively. Through thermodynamic modelling, Vetere et al. (2015) estimated the pre-eruptive temperature of latitic and rhyolitic magmas involved in the mixing process leading to the extrusion of the AD 1739 Pietre Cotte lava flow, obtaining temperature

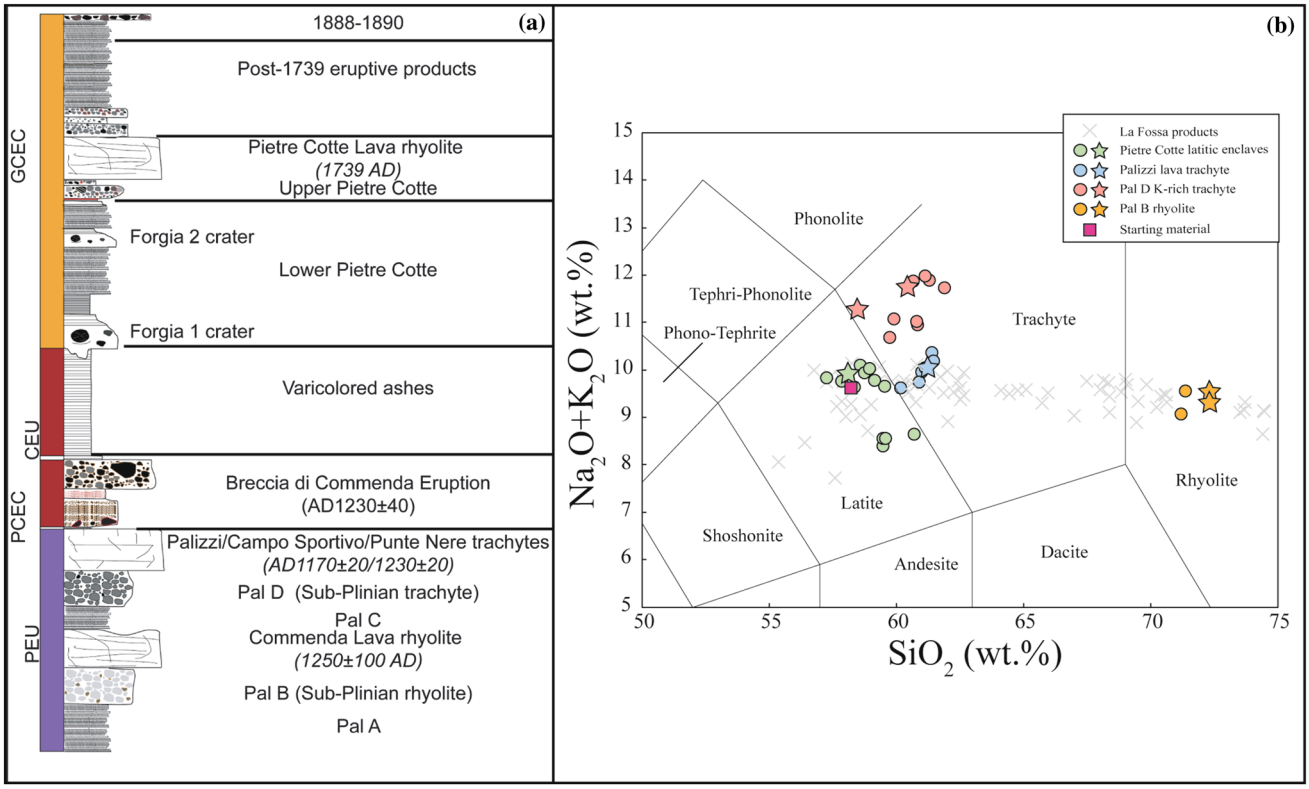

Fig. 2 **a** Stratigraphy of the deposits related to the last 1000 years of eruptive activity at La Fossa volcano (modified after Di Traglia et al. 2013); **b** total alkali vs SiO_2 diagram showing whole rock data of La Fossa products erupted in the last 1000 years (cross symbols: pyroclastic products and lava flows, literature data; filled circles: products belonging to the eruptive units investigated in this work, literature data; stars: new whole rock data). Major elements are recalculated to 100% on anhydrous basis. Literature data from Clocchiatti et al. (1994), Del Moro et al. (1998), De Astis et al. (2013), Nicotra et al. (2018) and Pinarelli et al. (2019)

of about 1010 °C for the latite and 950 °C for the rhyolite. In contrast, thermometric analyses on melt inclusions by Clocchiatti et al. (1994) indicate crystallization temperatures of 1100 ± 10 and 1050 ± 10 °C, respectively for the latite and trachyte involved in the AD 1888–1890 eruption. These values are in agreement with the temperature range 1000–1130 °C inferred by Bullock et al. (2019) for lati-trachytic magmas of Pietre Cotte, but is in excess compared to other recent temperature estimates for trachytic magmas of the recent activity (Palizzi, Pietre Cotte and AD 1888–1890) that indicate temperatures between 950 and 1000 °C (Fulignati et al. 2018; Masotta and Mollo 2019).

Materials and methods

Sampling

Samples were selected among the last 1000 years eruptive products of La Fossa, to cover the whole compositional spectrum of the erupted magmas. Samples from PCEC include the rhyolitic and trachytic pumices from the fallout layers (Pal B and Pal D, respectively) and the trachytic Palizzi lava flow. Samples from GCEC include the latitic enclaves contained in the obsidian of Pietre Cotte. The lava samples were prepared in thin sections for petrographic and microchemical analyses. The pumiceous lapilli were crushed and crystals with their host glass were manually separated under a stereomicroscope, embedded in epoxy mounts and polished for microanalysis. Sample powders were prepared by selecting aliquots of samples that did not show mixing features (e.g. compositional banding and enclaves), crushed and pulverized using a planetary mill at the Dipartimento di Scienze della Terra at the Università di Pisa and used for X-ray fluorescence (XRF) and ICP-MS analyses.

Temperature gradient experiments

Temperature gradient experiments were performed at the HP-HT Laboratory of Experimental Volcanology and Geophysics of Istituto Nazionale di Geofisica e Vulcanologia (Rome, Italy) in a non-end loaded piston cylinder (QUICKpress type), using a 19–25-mm assembly designed for experiments at pressure between 150 and 300 MPa

(Masotta et al. 2012a). Temperature gradient experiments take advantage of the intrinsic temperature gradient of piston cylinder furnaces. The temperature profile of the experimental assembly was previously measured by Masotta et al. (2012b). This experimental strategy has been adopted by several authors to investigate the effect of temperature gradient on melt differentiation, isotopic fractionation and fluid transport in magmas (Huang et al. 2009; Masotta et al. 2012b; Rodriguez et al. 2015; 2017; Laumonier et al. 2019). Experiments were performed at the pressure of 150 MPa, with temperature ranging from 1050 °C at the bottom of the capsule (hot spot) to 900 °C at the top, with constant run duration of 24 h. The temperature of the hot spot was constantly monitored using a C-type thermocouple, with a precision of 5 °C. At the beginning of the experiments, the temperature was increased to 1300 °C at a rate of 80 °C/min and held 30 min at this temperature, to anneal the crystal nuclei formed during the heating and to allow melt homogenization (Masotta et al. 2020). The temperature was then decreased to the experimental resting temperature with the same rate of 80 °C/min. Experiments were performed using 5 mm OD Pt capsules, at both anhydrous and hydrous ($H_2O = 2$ and 4 wt.%) conditions. Deionized H_2O was added in the hydrous charge using a micro-syringe, yielding a precision of about 0.1 wt.%. The weight of the capsule was checked before and after welding, and after 30 min at 110 °C to ensure that water did not escape during capsule preparation. As starting materials, we used a glass obtained by melting at 1400 °C for 1 h a latitic enclave from the AD 1739 Pietre Cotte lava flow (Table 1; Fig. 2b). This latitic composition represents one of the less evolved magma compositions erupted at La Fossa during the last 1000 years and taken as representative of the latitic magma of La Fossa plumbing system.

Analytical methods

The polished thin sections and resin mounts of natural products and the experimental samples were studied with a petrographic microscope, carbon-coated and analysed with a Quanta 450 Field Emission-Scanning Electron Microscope (FE-SEM) installed at the Centro Interdipartimentale di Scienza e Ingegneria dei Materiali (CISIM) at Università di Pisa. Backscattered electron (BSE) images were obtained using a 20 kV filament voltage and 10 mm working distance. The freeware software package ImageJ (Image Processing and Analysis in Java, https://rsb.info.nih.gov/ij/) was used for image analysis of experimental products to determine the glass/crystalline phase ratio and mineral phase abundance at different temperatures on BSE images of experimental products.

The whole rock major element chemical composition of natural samples was determined by X-ray fluorescence (XRF) on pressed powder pellets using an ARL 9400 XP + sequential X-ray spectrometer at Dipartimento di Scienze della Terra at the Università di Pisa. The loss on ignition (LOI) was determined at 950 °C. Trace element composition of the whole rock has been obtained through inductively coupled plasma-mass spectrometry (ICP-MS) analyses at the Dipartimento di Scienze della Terra at the Università di Pisa.

The chemical composition of the starting material glass, the experimental products and mineral phases of natural products was obtained using an electron probe

Table 1 Whole rock XRF analyses of the eruptive products of La Fossa and EPMA analysis of the glass used as starting material

Eruptive Unit	Pal D	Pal D	Pal B	Pal B	Pietre Cotte	Palizzi	Starting material	
Composition	K-rich trachyte	K-rich trachyte	Rhyolite	Rhyolite	Latite	Trachyte	Latite	
Type	Pumice	Pumice	Pumice	Pumice	Enclave	Lava	glass	σ (10)
SiO_2	57.58	59.52	69.21	70.03	57.21	60.70	56.60	0.47
TiO_2	0.66	0.69	0.17	0.19	0.41	0.50	0.40	0.04
Al_2O_3	18.27	18.52	13.06	13.36	20.36	16.73	19.98	0.49
Fe_2O_3*	5.89	4.25	2.33	2.31	5.53	4.80	5.95*	0.22
MnO	0.11	0.10	0.07	0.07	0.13	0.15	0.12	0.02
MgO	1.50	1.13	0.51	0.51	1.83	1.77	1.90	0.07
CaO	3.63	2.68	1.40	1.44	4.18	4.20	4.48	0.21
Na_2O	4.41	4.37	3.98	3.94	4.23	4.39	3.92	0.12
K_2O	6.65	7.22	5.07	5.04	5.63	5.60	5.32	0.22
P_2O_5	0.43	0.32	0.09	0.10	0.31	0.30	0.28	0.05
Total	99.13	98.80	95.89	96.99	99.82	99.14	98.95	
L.O.I	0.87	1.2	4.11	3.01	0.18	0.86	–	–

*Fe_2O_{3tot} for XRF analyses of natural products, FeO_{tot} for EPMA analysis of the starting glass

microanalyzer (EPMA) JEOL JXA-8200, operating in wavelength-dispersive mode at the Dipartimento di Scienze della Terra at the Università di Milano (operative conditions were 15 kV accelerating voltage, 10 nA beam current). Glasses in both natural and experimental products were analysed with a defocused electron beam of 5 µm and counting time of 5 s on background and 15 s on peak. For minerals, a beam size of 2 µm and counting time of 20 s on peaks and 10 s in background were used. The following standards have been adopted: jadeite (Si and Na), labradorite (Al and Ca), forsterite (Mg), andradite (Fe), rutile (Ti), orthoclase (K), barite (Ba), apatite (P) and spessartine (Mn). Na and K were analysed as first elements to minimize alkali loss. Energy-dispersive system (EDS) analyses were also performed with the Quanta 450 FE-SEM (20 kV filament voltage, 10 mm working distance) at CISIM at Università di Pisa.

In situ trace elements analyses of the cores and rims of mineral phases of natural products were performed by mean of laser ablation-inductively coupled plasma-mass spectrometry (LA-ICP-MS) at Géosciences Montpellier (University of Montpellier, AETE-ISO regional facility of the OSU OREME), with a pulsed 193-nm ArF excimer laser (Analyte G2 from Teledyne) coupled to a Thermofinnigan Element XR mass spectrometer. The laser was operated at a repetition rate of 8 Hz using spot sizes of 85 and 110 µm and a 6 J/cm^2 energy density. Total analysis time was 120 s with the first 80 s used for background measurement and last 40 s for sample ablation. Synthetic glass NIST 612 was used for external calibration. Accuracy of the analyses was monitored using the standard glass BIR-1 and SiO_2 for each sample used as internal standard. Data reduction was done with the software package Glitter (https://www.glitter-gemoc.com).

Results

Petrographic features and whole rock geochemistry

The recent activity of the PCEC and GCEC is characterized by the eruption of magmas that encompass a broad range of composition from latite to trachyte and rhyolite when considering the TAS diagram classification (Fig. 2b). For simplicity, we consider the petrographic and chemical features of selected samples that have been analysed in this study as representative of the occurrence of these three types of magmas in the stratigraphy of La Fossa. We focus on the enclaves of Pietre Cotte obsidian as representative of the latite (since most of the latitic products have been emplaced as fine-grained material, i.e. ashes), the Palizzi lava flow and Pal D fallout for the trachyte and the Pal B pumice for the rhyolite.

Latitic magma

The latitic magma occurs either as the juvenile component of several spatter and ash layers of PCEC and GCEC, and as magmatic enclaves in the rhyolitic pumices of Palizzi (Pal B), Pietre Cotte and in the rhyolitic obsidian lava flows of Commenda and Pietre Cotte (Perugini et al. 2007; Piochi et al. 2009; De Astis et al. 2013; Fig. 3a, b). The Commenda lava and the pyroclastic products of Pietre Cotte contain latitic magma both as vitrophyric bands stretched and mingled with the rhyolitic glass, and as rounded to blocky porphyritic enclaves with a microcrystalline groundmass. The latitic magma constituting the juvenile fraction of the pyroclastic deposits and that occurring as mingled bands is variably porphyritic (porphyritic index, P.I., ranging from 3 to 30%), whilst that constituting the enclaves in both lavas and pumices is crystal-rich (P.I. = 25–30%). The latitic enclaves sampled within the Pietre Cotte obsidian exhibit a mineral assemblage consisting of abundant euhedral to subeuhedral plagioclase (29%) and clinopyroxene (15%), olivine (3%) and rare sanidine (< 1%). Apatite and Ti-magnetite are common accessories. The groundmass is constituted by microlites of plagioclase and sanidine, and intergranular clinopyroxene and opaque minerals. Plagioclase and clinopyroxene phenocrysts often occur in glomerophyric texture (Fig. 3b). The bulk composition has SiO_2 ranging from 57 to 59 wt.% and $Na_2O + K_2O$ ranging from 8.5 to 10 wt.% (Table 1; Fig. 2b).

Trachytic magma

The trachytic magma is represented by several lava flows (Punte Nere, Palizzi, Campo Sportivo) and pyroclastic products of the PCEC (Di Traglia et al. 2013), as well as by some coarse ash layers and some pumice and bombs of the AD 1888–1890 eruption of GCEC (Clocchiatti et al. 1994). The trachytic magma also occurs as mingled bands within the rhyolitic pumices of the GCEC (Rossi et al. 2019). The Palizzi lava flow exhibits a porphyritic texture (P.I. ~ 20%) and a mineral assemblage made up of, in order of abundance, euhedral to subhedral plagioclase (12%), sanidine (10%), clinopyroxene (6%) and scarce (~ 1%) olivine (Fig. 3c). Glomerocrysts of plagioclase and clinopyroxene are also present. The groundmass is holocrystalline and made up by sanidine and minor amounts of plagioclase and clinopyroxene. The whole rock composition of Palizzi lava is trachytic with SiO_2 from 60 to 61 wt.% and $Na_2O + K_2O$ from 9.5 to 10.4 wt.% (Table 1; Fig. 2b). The pumices of Pal D fallout layer belonging to PCEC are highly vesiculated (~ 80 vol.%) and low porphyritic (P.I. is less than 5%). Scarce phenocrysts of plagioclase, clinopyroxene, sanidine, biotite and olivine occur in a glassy groundmass (Fig. 3d), whilst Ti-magnetite, apatite and pyrrhotite are common accessories (Fulignati

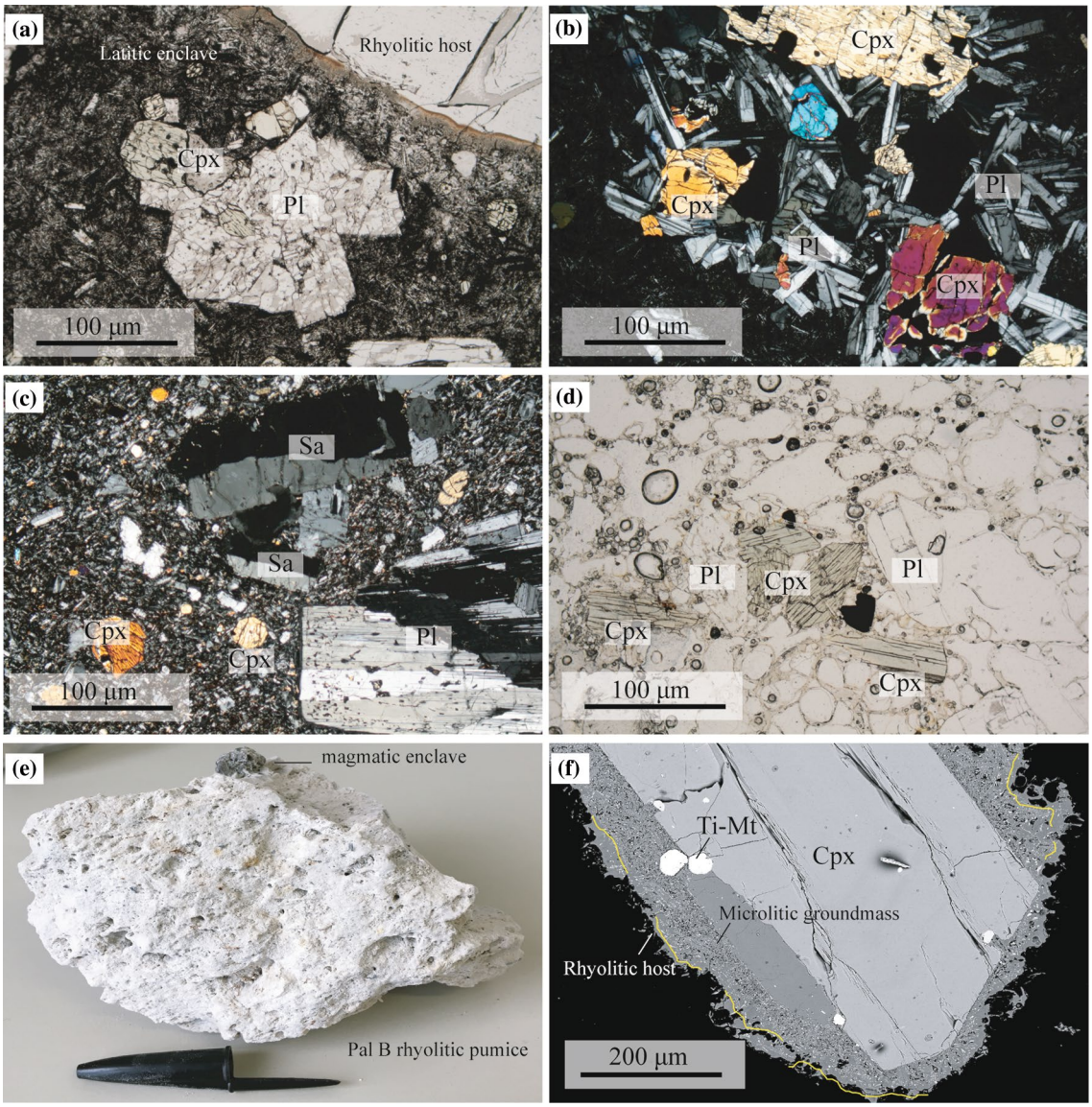

Fig. 3 Microphotographs of **a** a latitic crystal-rich enclave of Pietre Cotte and host rhyolitic lava flow, **b** a latitic crystal rich enclave of Pietre Cotte, **c** the Palizzi trachytic lava and **d** the K-rich Pal D pumice; **e** Pal B rhyolitic pumice with magmatic enclave; **f** BSE image of a clinopyroxene in the rhyolitic pumice of Pal B, the crystal is wrapped by a microlitic corona isolating it from the rhyolitic groundmass glass (yellow line). Mineral abbreviations: *Cpx* clinopyroxene, *Pl* plagioclase, *Sa* sanidine, *Ti-Mt* Ti-magnetite

et al. 2018). A K-rich trachytic composition is exclusive of the Pal D fallout layer. The SiO_2 content of these pumices ranges from 56 to 61 wt.%, with a K_2O content as high as 7.5 wt% and to a total alkali content up to 12 wt.% (Table 1; Fig. 2b).

Rhyolitic magma

The rhyolitic magma constitutes the juvenile fraction of both pyroclastic products (Pal B pumices, Pietre Cotte fallout and AD 1888–90 eruption bread crust bombs) and lava flows (Commenda and Pietre Cotte) of both PCEC and GCEC. All rhyolitic products exhibit evidence of mingling with either latitic or trachytic magmas, with the rhyolitic magma constituting the main fraction of the magma erupted during these eruptions. Rhyolitic products range from aphyric, with common xenocrysts of plagioclase and clinopyroxene (i.e. Pietre Cotte lava and pumices, AD 1888–90 eruption bread crust bombs; Piochi et al. 2009; De Astis et al. 2013) to weakly porphyritic (i.e. Pal B pumices). The pumices from the Pal B fallout deposit consist of white lapilli and bombs containing magmatic enclaves and showing a low porphyricity (P.I. is less than 5%) with a glassy groundmass (Fig. 3e). Phenocrysts are, in order of abundance, plagioclase, sanidine,

clinopyroxene and biotite. Accessory Ti-magnetite and apatite occur as inclusions within phenocrysts. The latitic and trachytic enclaves are constituted by phenocrysts of plagioclase and clinopyroxene that are surrounded by a dark microlitic matrix (Fig. 3f). The composition of these rhyolites range in SiO_2 from 71% to 72 wt.% and in $Na_2O + K_2O$ from 9.1 to 9.4 wt.% (Table 1; Fig. 2b).

Mineral chemistry of natural products

Plagioclase composition ranges from labradorite to andesine and oligoclase, with a significant overlap for latitic and trachytic products (Fig. 4a; Supplementary Material). In the latitic enclaves of Pietre Cotte, plagioclase is $An_{39–57}Ab_{37–48}Or_{5–13}$, whilst in the Palizzi trachytic lava and in the K-rich trachytic pumices (Pal D), plagioclase is $An_{39–61}Ab_{34–50}Or_{3–9}$ and $An_{37–55}Ab_{39–54}Or_{6–13}$, respectively. In contrast, in the rhyolitic pumices (Pal B), plagioclase is $An_{25–59}Ab_{33–66}Or_{3–11}$. Alkali feldspar shows a rather homogeneous composition in all products ($An_{1–6}Ab_{31–44}Or_{51–67}$), with the exception of the K-rich trachytic pumices (Pal D) that are evidently enriched in the Or component ($An_{3–5}Ab_{22–36}Or_{59–72}$).

Clinopyroxene has a rather similar augitic composition in all products ($Wo_{42–47}En_{37–42}Fs_{12–19}$), with the Diopside–Hedenbergite (DiHd) component ranging from 0.76 to 0.86 (Fig. 5; Supplementary Material). Clinopyroxene from the K-rich trachytic pumices of Pal D is enriched in the DiHd component (DiHd = 0.83–0.84) with respect to other latitic and trachytic products (DiHd = 0.76–0.82). In the rhyolitic pumices (Pal B), clinopyroxene displays a very large compositional variation (DiHd = 0.77–0.86). Biotite in the K-rich trachytic pumices of Pal D has Mg/(Mg + Fe) = 0.65–0.67 (Fulignati et al. 2018). Olivine compositions in the latitic and trachytic products varies from Fo_{72} to Fo_{55} (Gioncada et al. 1998).

Core and rim REE patterns in plagioclase reveal that the plagioclase of the K-rich trachytic pumices of Pal D has lower concentrations of HREE with respect to plagioclase of the latitic enclaves of Pietre Cotte and the trachytic lava of Palizzi (Fig. 6a; Supplementary Material). Sr and Ba abundances in plagioclase are higher in the K-rich trachytic pumices (Pal D) compared to the other latitic and trachytic magmas (Ba up to 2536 ppm and Sr up to 6869 ppm) and show a positive correlation with the Eu anomaly (Eu/Eu* = 7–28, with $Eu^* = (Sm_N - Gd_N)/2 + Gd_N$) (Fig. 6a). Clinopyroxene phenocrysts of Pal D show higher REE concentration compared to clinopyroxene of the latitic enclaves and the trachytic lava of Palizzi (Fig. 6b). The Sr content of clinopyroxene is variable (70–206 ppm), with the lowest values observed for the K-rich trachytic pumices of Pal D and a positive correlation with the Eu anomaly (0.47–0.72) (Fig. 6b; supplementary material).

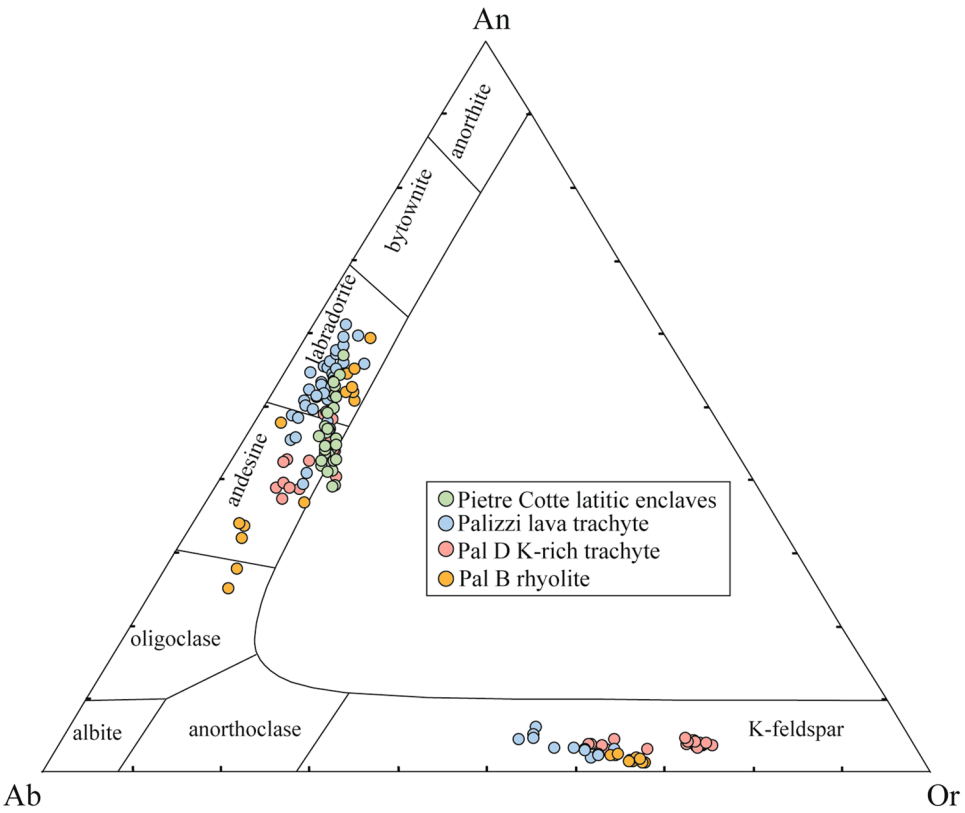

Fig. 4 Feldspar ternary diagram showing the composition of feldspar phenocrysts in the investigated products. Data of plagioclase occurring in the latitic enclaves of Pietre Cotte are from Piochi et al. (2009) and this work

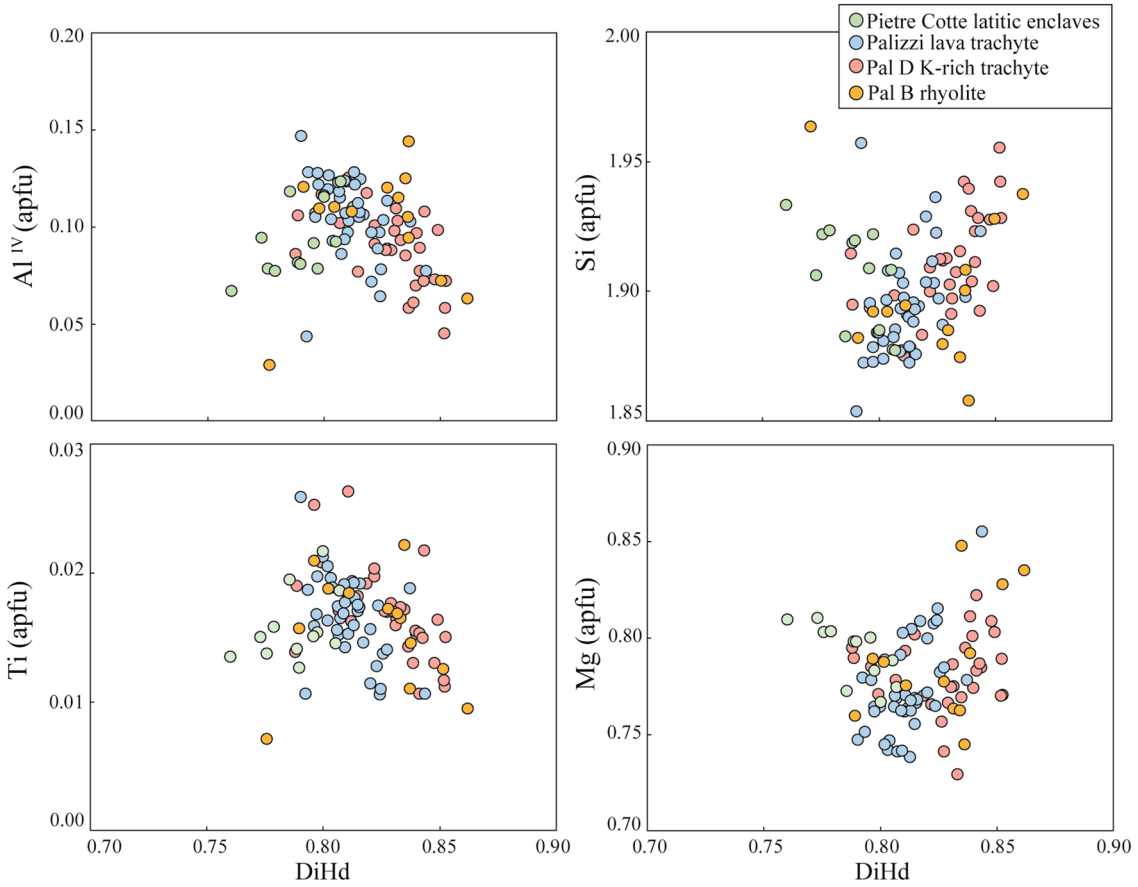

Fig. 5 Diagrams showing Al^{IV}, Si, Ti, Mg cations (apfu, atom per formula unit) vs. the DiHd component of clinopyroxene in the investigated products. Data of clinopyroxene occurring in the latitic enclaves of Pietre Cotte are from Piochi et al. (2009) and this work

Experimental results

Temperature gradient experiments produced variable phase relationships and crystal–melt proportion in response to the temperature variation along the charge (Table 2; Figs. 7, 8). In all the experiments, clinopyroxene is the most abundant mineral phase, forming large (200–1000 μm) skeletal crystals in the hotter region of the capsule and small (20–200 μm) and increasingly euhedral crystals at lower temperatures. Such variability of crystal size and shape can be attributed to the effect of undercooling upon cooling from superliquidus (Shea and Hammer 2013; Pontesilli et al. 2019; Masotta et al. 2020). At anhydrous conditions ($H_2O = 0$ wt.%), clinopyroxene is the only mineral in the temperature range 1050–1000 °C. Fe-oxide and alkali feldspar start to crystallize at 1000 °C. The same mineral assemblage constituted by clinopyroxene, Fe-oxide and alkali feldspar is maintained up to the top of the capsule, where the crystal fraction increases up to 80 vol.% at about 900 °C (Table 2; Fig. 8). Upon increasing crystallization, the composition of the interstitial glass enriches in K_2O from 6.0 to 7.3 wt.% with only a slight variation in SiO_2 from 58 to 59 wt.% (Fig. 9; Supplementary Material). It is worth noting that the glass in the anhydrous experiment is slightly enriched in FeO compared to the starting material, as result of the extensive crystallization of feldspar (Fig. 9). At hydrous conditions with $H_2O = 2$ wt.% and at the temperature of 1050 °C, clinopyroxene and Fe-oxide co-saturate the melt. Biotite crystallization starts at 1000 °C and is followed by the crystallization of plagioclase and alkali feldspar at 925 °C. At the top of the capsule, the temperature decreases to 900 °C and the crystallinity reaches ~ 50 vol.% (Table 2; Fig. 8). The composition of interstitial glasses along the experimental charge varies with the increasing crystallization, with SiO_2 increasing from 58 to 62 wt.% and K_2O increasing from 5.7 to 6.7 wt.% (Fig. 9; supplementary material). In the hydrous experiment with $H_2O = 4$ wt.%, clinopyroxene, biotite and Fe-oxide co-saturate the melt in the temperature range 1050–1000 °C and the same mineral assemblage is maintained up until the temperature of 900 °C, where the crystallinity is ~ 40 vol. % (Table 2; Fig. 8). The composition of interstitial glass varies in SiO_2 from 62 to 67 wt.%, with a rather small increase in K_2O from 5.4 to 6.1 wt.% and a marked depletion in FeO, CaO and MgO due to

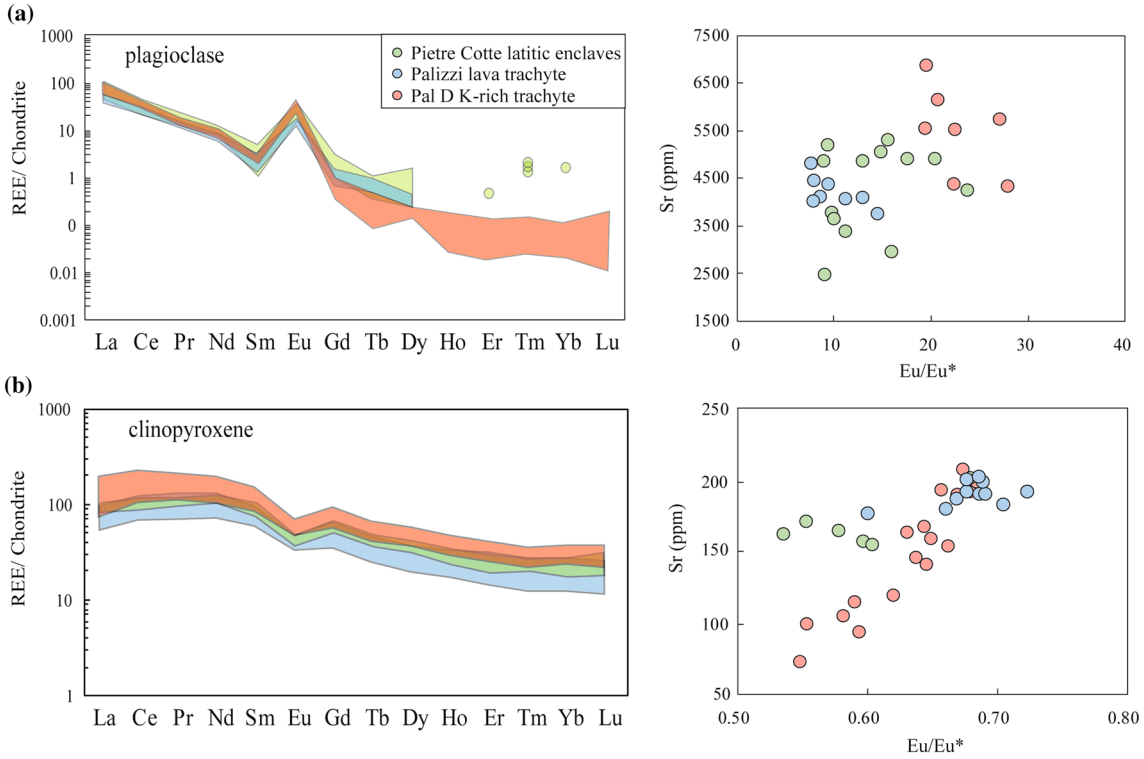

Fig. 6 Chondrite-normalized rare earth element (REE) patterns and Sr vs. Eu/Eu* for **a** plagioclase and **b** clinopyroxene. Data of plagioclase in the latitic enclaves of Pietre Cotte and Palizzi lava flow are from Piochi et al. (2009), Nicotra et al. (2018) and this work. Data of clinopyroxene in the latitic enclaves of Pietre Cotte are from Piochi et al. (2009)

Table 2 Phase proportions in experimental samples obtained through image analysis

Phase (vol.%)	Temperature along the capsule (°C)					
	1050–1025	1025–1000	1000–975	975–950	950–925	925–900
$H_2O = 0$ wt.%						
Glass	86	84	61	45	30	20
Cpx	14	16	14	24	26	24
Afs	0	0	24	30	42	54
Ox	0	0	1	1	2	2
$H_2O = 2$ wt.%						
Glass	90	87	82	77	68	50
Cpx	8	11	14	17	19	24
Afs + Pl*	0	0	0	0	0	15
Ox	1	1	1	1	2	2
Bt	0	0	2	2	8	6
Vesicles	1	1	1	3	3	3
$H_2O = 4$ wt.%						
Glass	80	78	72	69	65	60
Cpx	6	7	13	13	13	15
Ox	1	1	1	2	2	2
Bt	9	10	10	12	15	18
Vesicles	4	4	4	4	5	5

*Alkali feldspar and plagioclase counted together because of the similar BSE intensity

Cpx clinopyroxene, *Afs* alkali feldspar, *Pl* plagioclase, *Ox* oxide, *Bt* biotite

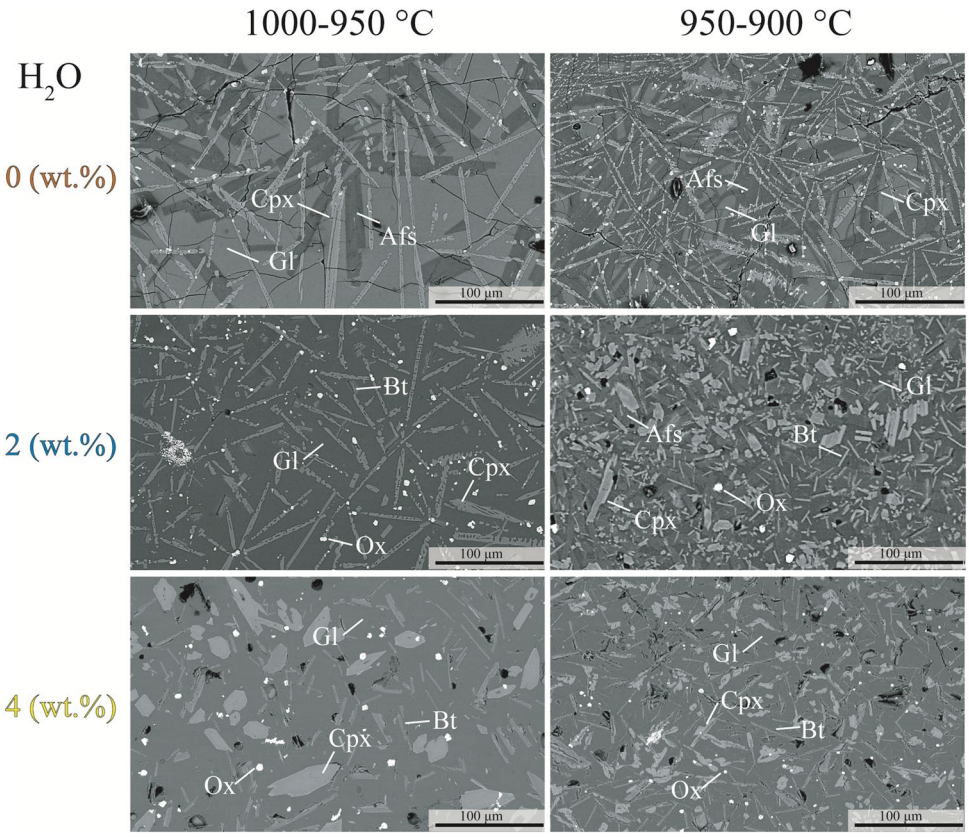

Fig. 7 BSE images of experimental products at different temperature ranges and H_2O content. Phase abbreviations: *Cpx* clinopyroxene, *Afs* alkali-feldspar, *Bt* biotite, *Ox* oxide, *Gl* glass

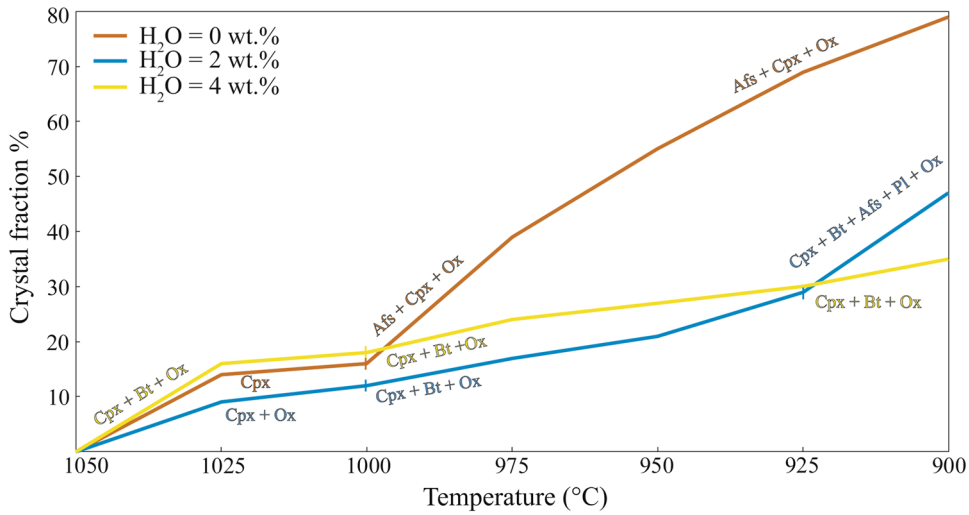

Fig. 8 Crystallinity variation along the temperature gradient of the experiments. Phase abbreviations: *Cpx* clinopyroxene, *Afs* alkali-feldspar, *Bt* biotite, *Pl* plagioclase, *Ox* oxide

extensive crystallization of biotite and clinopyroxene (Fig. 8; Supplementary Material).

Thermo-barometry and hygrometry

Crystallization temperature and pressure of products representative of the latitic and trachytic magmas of PCEC (K-rich trachytic pumices of Pal D and trachytic lava flow of Palizzi) and GCEC (latitic enclave of Pietre Cotte lava flow) were estimated using the clinopyroxene–liquid thermo-barometer of Masotta et al. (2013). This model is specific to alkaline-differentiated magmas and includes in the calibration dataset experiments performed with the trachytic composition of the Palizzi lava flow. The use of this model theoretically yields to the highest accuracy for the estimates of the intensive variables of magmas erupted at La Fossa (Table 3). Equilibrium clinopyroxene–liquid pairs

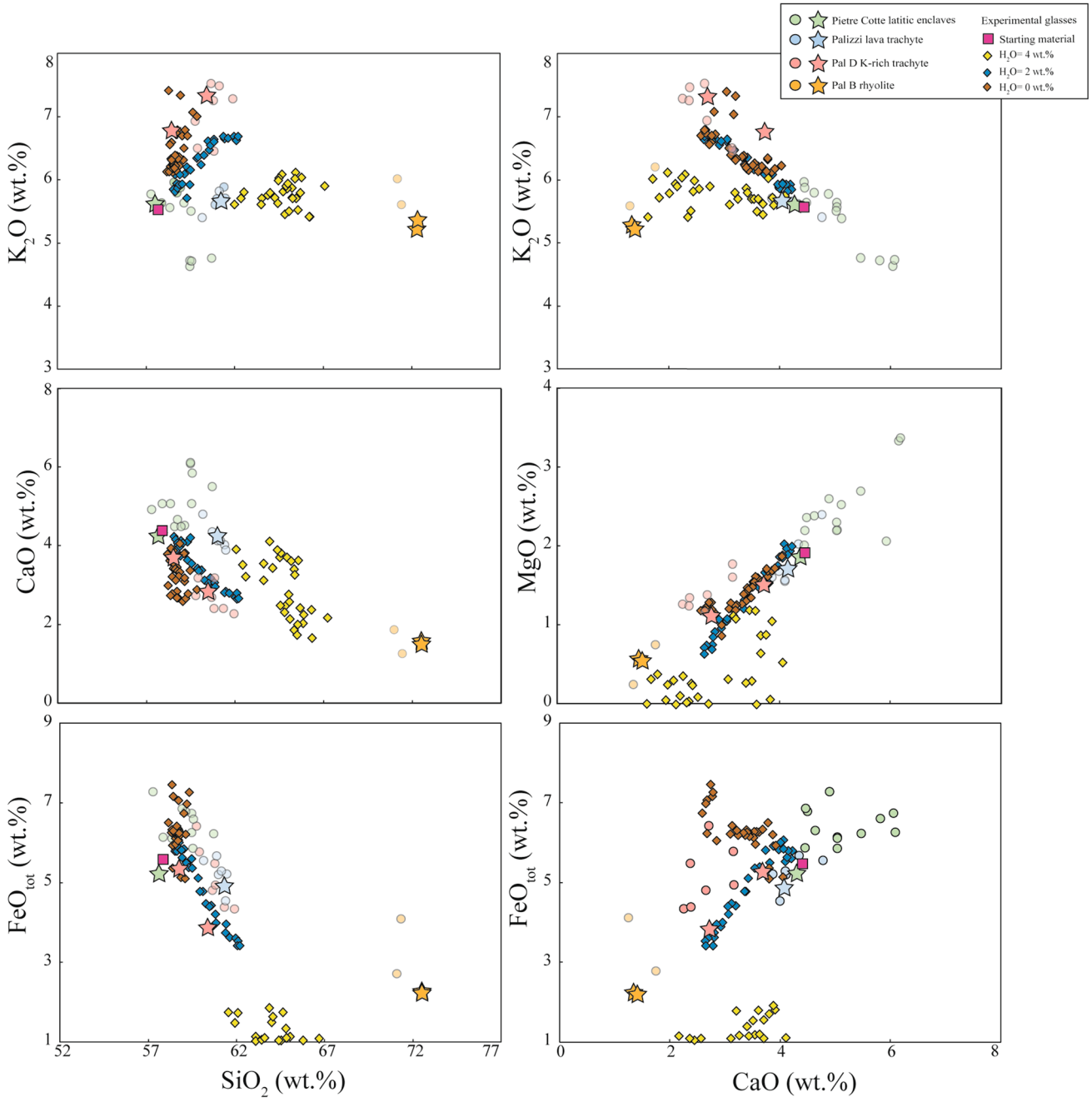

Fig. 9 Major elements variation diagrams of La Fossa products (symbols and references as reported in Fig. 2b) and experimental glasses. Major elements are recalculated to 100% on anhydrous basis

were selected using the DiHd equilibrium model of Mollo et al. (2013), assuming at equilibrium clinopyroxene showing a ΔDiHd (predicted vs. calculated DiHd component in clinopyroxene) of less than 0.1 (Mollo and Masotta 2014; Fig. 10a). Most of the clinopyroxene crystals resulted in equilibrium with the latitic and trachytic magmas, with the exception of clinopyroxene in the rhyolitic pumices of Pal B, not used for the calculation of the intensive variables (Fig. 10a). Given the lack of glass in the trachytic lava flow (Palizzi) and the latitic enclave (Pietre Cotte), the bulk rock composition was assumed as representative of the liquid in equilibrium with clinopyroxene. For the K-rich trachytic pumices of Pal D, where the matrix glass was available, we paired crystal cores with the bulk rock and melt inclusion analyses and the crystal rims with matrix glass analyses (data from Fulignati et al. 2018). The H_2O value used as input for the thermo-barometer was assumed between 2.0 and 3.5 wt.%, as determined through iterative solution by

Table 3 Temperature, pressure and H_2O estimates for the investigated products of La Fossa

Eruptive Unit		Pietre Cotte	Pal D	Palizzi	Pal B
Composition		Latite	K-rich trachyte	Trachyte	Rhyolite
Type		Enclave	Pumice	Lava	Pumice
T (°C)	Cpx-liq (cores)[a]	1027 ± 5	1004 ± 14	1007 ± 9	–
	Cpx-liq (rims)[a]	1025 ± 6	996 ± 13	1005 ± 8	–
	REE in Cpx-Pl[b]	1037 ± 8	991 ± 31	1057 ± 8	–
	Pl-liq[c]	–	–	–	952 ± 7
P (MPa)	Cpx-liq (cores)[a]	307 ± 47	160 ± 54	199 ± 39	–
	Cpx-liq (rims)[a]	294 ± 38	132 ± 33	208 ± 30	–
H_2O (wt.%)	Pl-liq[d]	2.50–3.50[e]	2.54 ± 0.57	2.50–3.50[e]	1.99 ± 0.30

*Data from Masotta and Mollo (2019)

[a]Masotta et al. (2013)

[b]Sun and Liang (2017)

[c]Putirka (2008)

[d]Masotta and Mollo (2019)

combining the plagioclase–liquid hygrometer of Masotta and Mollo (2019) and the clinopyroxene–liquid thermo-barometer of Masotta et al. (2013). We note that to an increase of the H_2O content of 1 wt.% corresponds to an increase of the temperature estimates of less than 10 °C.

Pressure and temperature values calculated for the trachytic K-rich Pal D pumices are based on 30 core–liquid pairs and 20 rim–liquid pairs. The cores indicate crystallization temperature and pressure of 1004 ± 14 °C and 160 ± 54 MPa, while crystal rims show slightly lower values of temperature and pressure of 996 ± 13 °C and 132 ± 33 MPa (Fig. 10b). Clinopyroxene core–liquid pairs (20 pairs) from the trachytic lava flow of Palizzi indicate temperature and pressure of 1007 ± 9 °C and 199 ± 39 MPa, whereas rim–liquid pairs (20 pairs) give temperature and pressure of 1005 ± 8 °C and of 208 ± 30 MPa (Fig. 10b). Notably, the estimates obtained using both core and rim analyses are identical within the error. Compared to the trachytic products, the clinopyroxene–liquid pairs of the latitic enclave of Pietre Cotte lava flow indicate higher temperature and pressure, with core–liquid pairs (10 pairs) giving values of 1027 ± 5 °C and 307 ± 47 MPa and rim–liquid pairs (10 pairs) yielding to values of 1025 ± 6 °C and 294 ± 38 MPa (Fig. 10b). As for the trachytic lava of Palizzi, core and rim analyses give results that are identical within the error. Overall, the temperature and pressure distribution inferred using clinopyroxene-liquid thermo-barometry (Fig. 10b) is consistent with the polybaric nature of the plumbing system of La Fossa, with latitic magmas evolving at greater depth compared to trachytic ones.

Further calculation of the crystallization temperatures for the latitic and trachytic magmas at La Fossa has been done using the REE-in-plagioclase–clinopyroxene thermometer (Sun and Liang 2017). This thermometer is based on REE + Y exchange between plagioclase and clinopyroxene. Calculations have been performed assuming pressures of 150 and 300 MPa, and H_2O contents of 2.5 and 3.0 wt.%, for the K-rich trachytic pumices of Pal D and the latitic enclave of Pietre Cotte obsidian, respectively. The results, based on 42 clinopyroxene–plagioclase pairs (14 pairs for each magma composition), indicate average temperatures of 991 ± 31 °C and 1037 ± 8 °C for the Pal D K-rich trachytic pumices and the Pietre Cotte latitic enclave, respectively (Table 3; Fig. 10c, d). These values are consistent with those inferred using the clinopyroxene–liquid thermo-barometer. In contrast, the average temperature obtained for the Palizzi trachytic lava is slightly higher (1057 ± 8 °C), probably testifying to a higher co-saturation temperature for clinopyroxene and plagioclase.

Plagioclase–liquid pairs have been used to determine the H_2O content of the K-rich trachytic magma of Pal D eruption, through the plagioclase–liquid hygrometer of Masotta and Mollo (2019). Plagioclase core analyses coupled with the whole rock compositions yield a H_2O content of 2.54 ± 0.57 wt.%, whilst rim analyses coupled with the average composition of the matrix glass indicate a water content of 2.42 ± 0.52 wt.%. These values are in accordance with those proposed for the latitic and trachytic magmas at La Fossa by Masotta and Mollo (2019), and with the highest water content measured in melt inclusions hosted in the Pal D phenocrysts (ranging from 1.01 to 2.52 wt.%, with the low measured values interpreted as degassed hourglass inclusions; Fulignati et al. 2018).

The crystallization temperature of the Pal B rhyolite was estimated using the plagioclase–liquid thermometer (Putirka 2008), using the plagioclase occurring in the Pal B pumices and the bulk rock analyses as representative of the liquid in equilibrium. Pressures of 100 and 200 MPa were used for

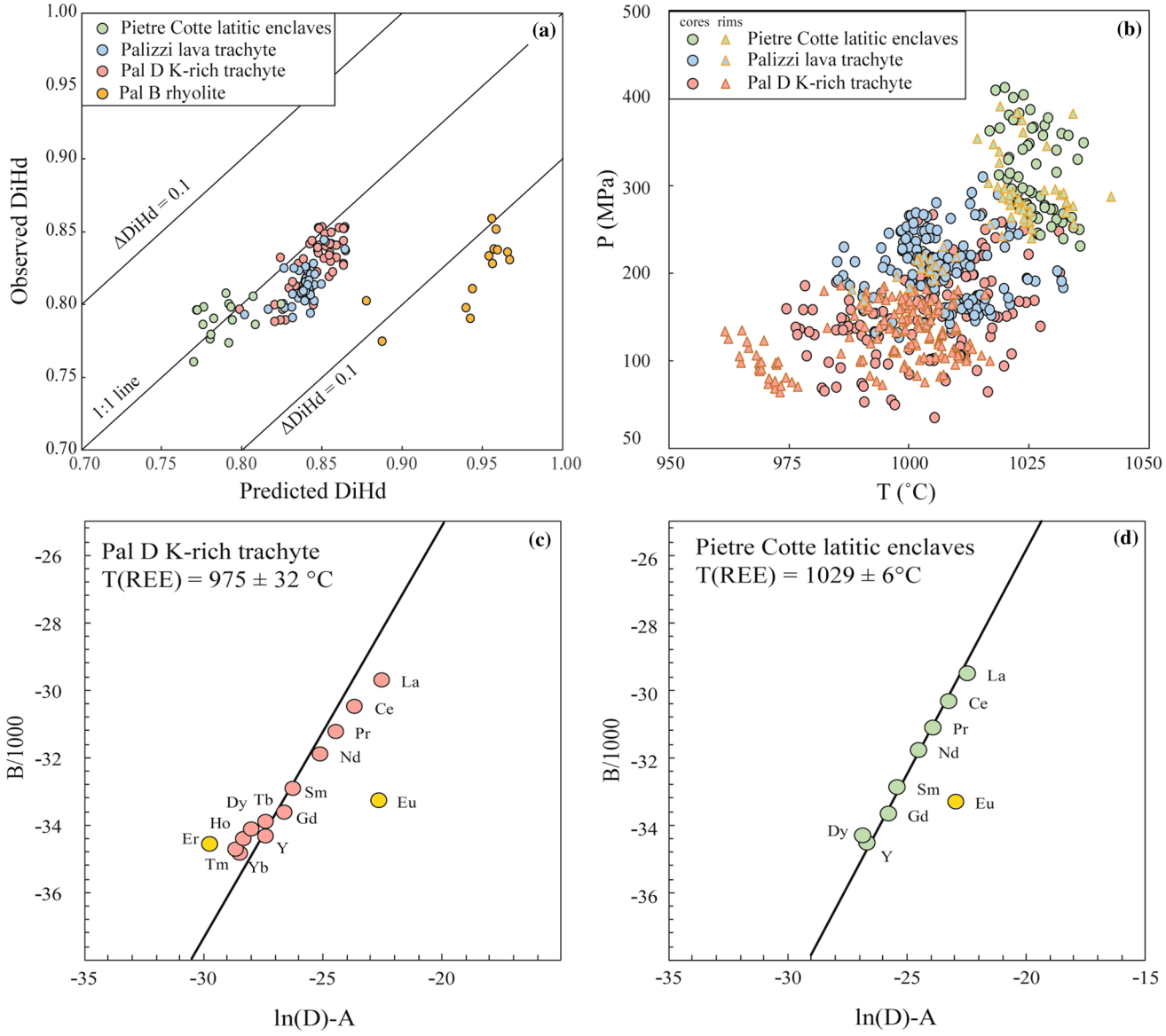

Fig. 10 **a** Test of equilibrium for clinopyroxene comparing the observed and predicted values for DiHd component in clinopyroxene; **b** pressure and temperature estimates for the latitic and trachytic magmas at La Fossa obtained through clinopyroxene–liquid thermobarometer of Masotta et al. (2013); **c**, **d** temperature inversion diagrams showing the linear least squares regression analyses of the REE partitioning data calculated for plagioclase–clinopyroxene pairs from Pal D K-rich pumice and Pietre Cotte latitic enclave using the REE-exchange thermometer of Sun and Liang (2017). D is the partition coefficient of a given element in the geochemical group of REE. A and B are coefficients corresponding to the changes of entropy and enthalpy. At the thermodynamic equilibrium, all elements in the same geochemical group define a straight line (best fit line passing through the origin) in a plot of ln (D) – A vs. B/1000, where temperature corresponds to the slope. Yellow dots are the data excluded from the regression analysis

calculation, yielding to comparable crystallization temperatures of 952 ± 7 °C and 957 ± 8 °C, respectively (Table 3). All the considered plagioclase–liquid pairs provide values of K_D (Ab − An) of 0.04–0.12, consistent with the equilibrium value of 0.10 ± 0.05 (Putirka 2008). The same plagioclase–liquid pairs, along with the inferred temperatures, have been used in the hygrometer of Masotta and Mollo (2019) to determine the H_2O content of the rhyolitic magma of Pal B pumices, obtaining values of 1.99 ± 0.30 wt.% H_2O.

Discussion

Magma crystallization conditions

A polybaric plumbing system consisting of multiple storage levels with magma batches undergoing mutual interactions has been invoked to explain the broad range of magma composition and the variety of mixing and mingling features observed in the eruptive products at La Fossa volcano

(Peccerillo et al. 2006; Piochi et al. 2009; De Astis et al. 2013; Paonita et al. 2013; Vetere et al. 2015; Mandarano et al. 2016; Nicotra et al. 2018; Bullock et al. 2019). In spite of the number of studies, a large uncertainty of crystallization pressure and temperature estimates of magmas erupted at La Fossa volcano still exists. This is mostly related to the reduced accuracy of several thermo-barometric models applied to alkaline magma compositions and the lack of equilibrium selection criteria. Indeed, it has been demonstrated that thermo-barometric and hygrometric models that are based on calibration specific to a restricted range of magma compositions have lower uncertainties compared to models based on global regressions (Masotta et al. 2013; Mollo et al. 2015; Perinelli et al. 2016; Brugman and Till 2019). Coherent with previous works, our estimates envisage a polybaric storage system below La Fossa cone but, in addition, they allow to precisely define the difference in the crystallization pressure between the K-rich trachytic magma of Pal D and the other trachytic magmas (Fig. 2b). The K-rich trachytic magma of Pal D pumices equilibrated at a lower pressure (160 ± 54 MPa) compared to other trachytic (208 ± 30 MPa) and latitic (307 ± 47 MPa) magmas (Fig. 10b). The lowermost pressure obtained for the K-rich trachytic magma of Pal D (30–50 MPa) is consistent with the minimum H_2O saturation pressure estimated by Fulignati et al. (2018) based on the H_2O content in melt inclusions. We, therefore, suggest that the K-rich trachytic magma feeding the Pal D eruption was erupted from a reservoir located at shallower depth (1–3 km) compared to those feeding the other latitic and trachytic eruptions (3–8 km).

As regarding the rhyolitic magma of Pal B, the inferred temperature of $\sim 955 \pm 8$ °C is fully consistent with the temperature estimate of 950 °C inferred for the GCEC rhyolites (Vetere et al. 2015). The lack of clinopyroxene in equilibrium with the rhyolite (Fig. 10a) did not allow a reliable pressure estimate for the rhyolitic magma; however, based on the low H_2O content of the rhyolite (~2 wt.%), we can infer a H_2O-saturation pressure below 100 MPa.

The crystallization conditions obtained in this study reinforce the evidence of the capability of the shallow magma system of La Fossa to feed also significant explosive eruptions. Indeed, the rhyolitic Pal B and K-rich trachytic Pal D eruptions constitute the main explosive events occurred at La Fossa volcano during the studied period, being characterized by similar plume height (7–8 km a.s.l.) and erupted volume ($3.6–4.0 \times 10^6$ m^3) (Biass et al. 2016).

Magma differentiation modelling

One of the most interesting features at la Fossa volcano is the twofold differentiation path followed by intermediate magmas during their late evolution, leading to the formation of either K-rich trachytes (represented by Pal D pumices) or trachytes (the trachytic lava flows of Palizzi, Punte Nere and Campo Sportivo) and then rhyolites (represented by the obsidian lava flows of Commenda and Pietre Cotte or by the pumices of Pal B) (Fig. 2b). A combination of fractional crystallization and crustal assimilation (AFC) processes has been invoked to explain the formation of the rhyolitic magmas starting from the less differentiated latitic ones (Clocchiatti et al. 1994; Del Moro et al. 1998; Piochi et al. 2009; Pinarelli et al. 2019; Bullock et al. 2019). The low content of Ba and Sr, and the negative Eu anomaly of the Pietre Cotte rhyolitic lava testifies to a process of fractional crystallization with a significant involvement of plagioclase and K-feldspar (Piochi et al. 2009). In this framework, we explored what processes determined the enrichment in K_2O that produced the K-rich trachytic magma and the differentiation to trachytes and rhyolites. We thus performed mass balance calculations using major element composition of bulk rocks and minerals, starting from the latitic magma (latitic enclave of Pietre Cotte obsidian) and targeting the composition of both the trachytic (i.e. the K-rich trachyte of Pal D pumices and the trachyte of the Palizzi lava) and the rhyolitic (i.e. Pal B pumice) magmas. The choice of the latite as starting point for the differentiation modelling is supported by the fact that this composition represents: (i) one of the least evolved intermediate magmas erupted at La Fossa and (ii) the point in the differentiation line where two distinct evolutionary trends branch out (Fig. 2b). Four possible differentiation segments are thus modelled (Fig. 11):

1. *Latite to K-rich trachyte* The K-rich trachytic composition of Pal D pumices is obtained through fractionation (~31%) of a mineral assemblage made up by plagioclase (17%), clinopyroxene (7%), sanidine (4%), Fe–Ti oxide (2%), olivine (1%) and biotite (0.5%).
2. *Latite to trachyte* The trachytic composition of the Palizzi lava is obtained through fractionation (~38%) of a mineral assemblage made up by sanidine (14%), plagioclase (13%), clinopyroxene (5%), biotite (1%), Fe–Ti oxide (3%) and olivine (~1%).
3. *K-rich trachyte to rhyolite* the rhyolitic composition of Pal B pumices is obtained through fractionation (~68%) of a mineral assemblage made up by sanidine (39%), plagioclase (19%), biotite (6%), Fe–Ti oxide (4%) and clinopyroxene (1%).
4. *Trachyte to rhyolite* The rhyolitic composition of Pal B pumices is obtained through fractionation of a mineral assemblage (~62%) made up by sanidine (26%), plagioclase (24%), clinopyroxene (5%), Fe–Ti oxide (4%) and biotite (3%).

Concerning the differentiation toward the two trachytic terms (hereafter referred to K-rich and normal trachytes), segments 1 and 2 differ substantially in the proportions of

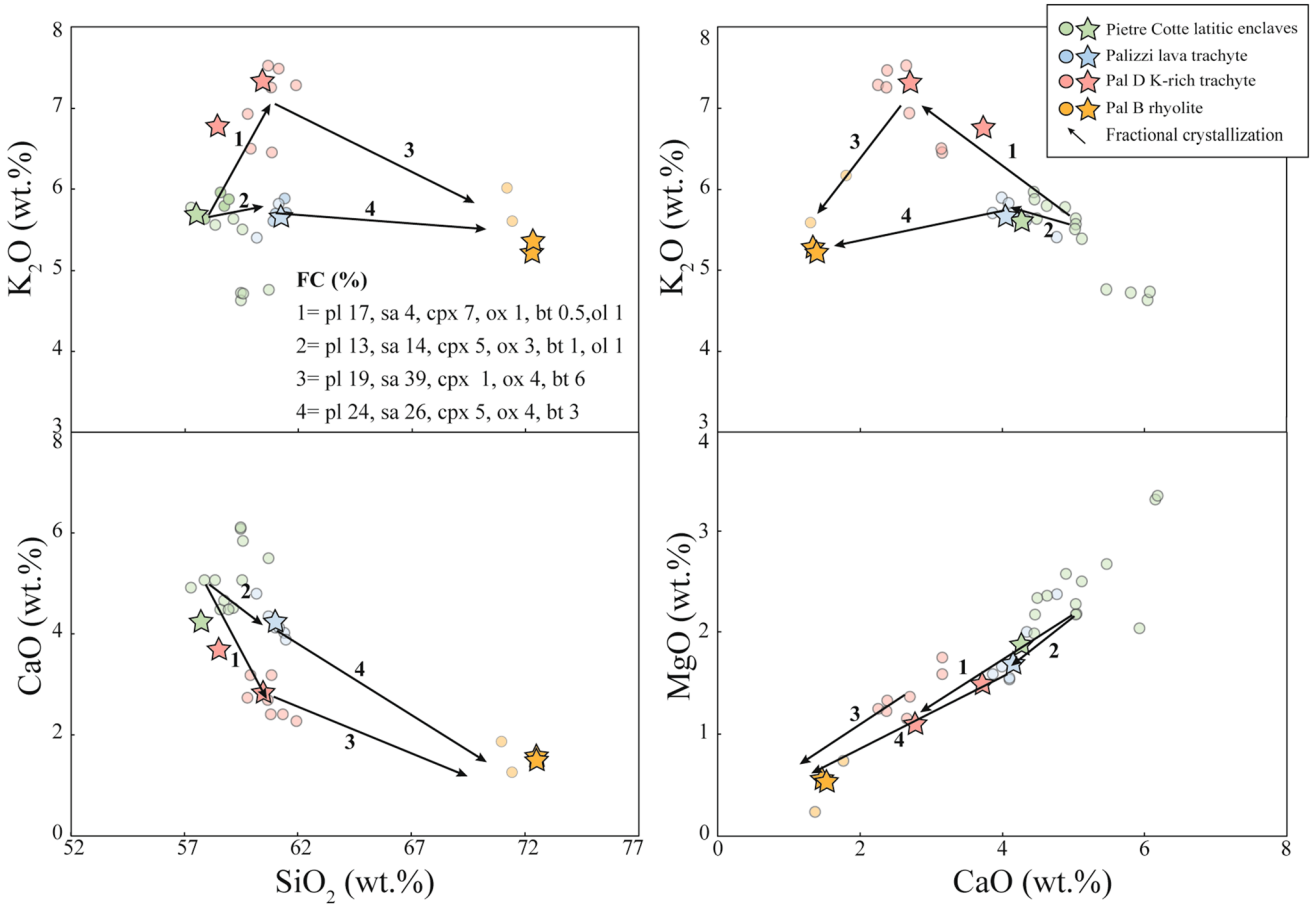

Fig. 11 Fractional crystallization modelling based on mass balance calculation using major element of bulk rocks and mineral of the eruptive products of La Fossa (symbols and references as reported in Fig. 2b). The starting composition is represented by the latitic enclaves of Pietre Cotte, whereas the target compositions are the K-rich trachyte of Pal D (segment 1), the trachyte of the Palizzi lava (segment 2) and the rhyolite of Pal B (segments 3 and 4). Only compositions displaying a sum of squared residual (SSR) below 2 were considered

fractionated mineral phases. The plagioclase/sanidine ratio varies from about 4:1 to about 1:1, determining the evolution of the melt toward either K-rich (segment 1) or normal (segment 2) trachytes (Fig. 11). The two contrasting trends can be associated to the different pressures inferred from thermo-barometric calculation, suggesting a lower pressure for the K-rich trachyte compared to normal trachyte. Indeed, the higher fractionation of plagioclase would be favoured at a lower pressure due to the lower activity of H_2O in the melt. This is supported by the higher Eu anomaly and Sr concentration of plagioclase in the K-rich trachytes of Pal D pumices compared to plagioclase of the Palizzi lava trachyte (Fig. 6a). The formation of the rhyolite has been modelled by considering differentiation paths starting from both K-rich and normal trachytes (segments 3 and 4, respectively; Fig. 11). Segment 3 differs from segment 4 because of the higher plagioclase/sanidine ratio (about 2:1 against about 1:1) and the higher biotite/clinopyroxene ratio (about 6:1 against about 1:2). The compositional variability of magmas erupted at La Fossa (Fig. 2b), with the K-rich trachytic composition being observed only in a single eruptive event (Pal D pumices), overall suggests that rhyolitic magmas originated through differentiation of normal trachytes. This is supported by the lack of solid enclaves enriched in biotite with respect to clinopyroxene and by the higher pressure estimates for the normal trachytes, compared to the K-rich one.

In addition to the mass balance calculations using major elements, we modelled the evolution of latitic and trachytic magmas using assimilation + fractional crystallization (AFC) trace elements modelling (see Supplementary Material for the used parameters). Some extent of crustal assimilation has been invoked to explain the complex evolution of magmas erupted at La Fossa volcano, through the interaction with crustal rock of the Calabro Peloritano basement (Frezzotti et al. 2004; Piochi et al. 2009; De Astis et al. 2013). Hence, starting from the same latitic composition and assuming the same phase assemblage obtained through mass balance

calculations, the formation of the rhyolitic magma (Pal B pumices) is entirely explained by 50–60% crystal fractionation with an assimilation rate between 0.2 and 0.5 (Fig. 12). This calculation also shows that the trachytic products are better explained by low degrees of fractional crystallization, whilst assimilation becomes increasingly important during the late evolution to rhyolites, as suggested by Del Moro et al. (1998). In contrast, the origin of the K-rich trachytic magma is explained by 30–40% crystal fractionation involving a higher plagioclase/sanidine ratio in the fractionated solid and leading to an increase in Ba (Fig. 12).

Temperature gradient experiments explored the effect of the H_2O content (0, 2 and 4 wt.%) on the differentiation of the latitic magma, designating different paths of melt differentiation that overall indicate an increase of the SiO_2/K_2O ratio with the increasing H_2O in the system (Fig. 9). The interstitial glasses analysed in the two experiments with 0 and 2 wt.% H_2O better approximate the K_2O enrichment trend modelled by segment 1 (K-rich trachytes), whereas the most hydrous experiment with 4 wt.% H_2O approximates the SiO_2 enrichment trend modelled by segments 2 and 4 (trachytes and rhyolites). Overall, the divergence of these trends is explained by the different proportion of feldspars, clinopyroxene and biotite that crystallize at different H_2O content (see Table 2). Therefore, in ultimate analysis, experimental results confirm what inferred from the differentiation modelling and from thermo-barometric analyses, that the K-rich trachytic magma of Pal D originated at lower pressure and at lower H_2O concentration compared to other trachytic magmas erupted at La Fossa volcano. More than other parameters, the H_2O content in the melt (in turn related to the storage depth of the magma), by varying the clinopyroxene/feldspar + biotite ratio, exerts a primary control on phase stability and determines the differentiation trend towards either K-rich trachytes (segment 1) or trachytes and rhyolites (segments 2 and 4). The higher H_2O content of both latitic and trachytic magmas, compared to the K-rich trachytic one, is in accordance with the H_2O estimates of 2.5–3.5 wt.% inferred using the plagioclase–liquid hygrometer (Masotta and Mollo 2019). This finding is in accordance with experimental results by Beermann et al. (2017), reproducing the crystallization of basaltic andesite of the 24 ka Lower Pollara eruption (Salina, Aeolian Islands) and demonstrating that a strong increase of K_2O relative to SiO_2 can be reproduced at higher temperatures and relatively low H_2O content.

The role of crystal mushes within La Fossa plumbing system

Using mass balance calculations and AFC modelling on major and trace elements, we showed that rhyolitic magmas are produced from an initial latitic composition by a minimum of 60% of crystal fractionation (Figs. 11 and 12). The low porphyritic or even aphyric nature of the rhyolitic magmas erupted at La Fossa is in contrast with this result and other possibilities regarding the formation of crystal-poor differentiated magmas must be considered.

The origin of the crystal-poor rhyolites by partial melting of subvolcanic rocks favoured by the intrusion of hotter

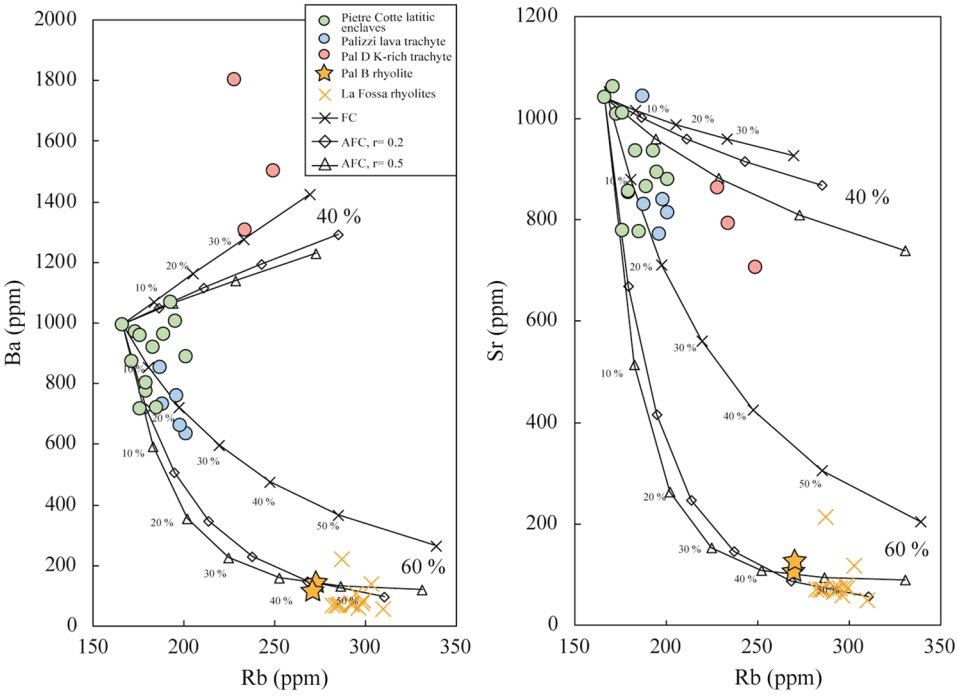

Fig. 12 **a** Assimilation and fractional crystallization (AFC) trace element modelling (symbols as reported in Fig. 2b). *r* is the assimilation rate/fractionation rate. See Supplementary Material for the parameters used in the model and for ICP-MS analyses of the Pal B rhyolite. Literature data from De Astis et al. (2013), Nicotra et al. (2018), Bullock et al. (2019) and Pinarelli et al. (2019)

magmas at depth, as proposed by Masotta et al. (2018) for the formation of rhyolitic melts at Krafla volcano (Iceland), can be ruled out since the lithology of the subvolcanic rocks are inconsistent with the formation of rhyolitic melts. The perforations carried out for geothermal exploration within the La Fossa Caldera at 1000 m and 2000 m revealed the presence of latitic-shoshonitic subvolcanic bodies, as well as a monzogabbroic body (Faraone et al. 1986; Gioncada and Sbrana 1991), which could be consistent with the variety of enclaves contained in the rhyolitic products but not with the origin of the rhyolite itself. The rather homogeneous composition of the rhyolitic magmas erupted at La Fossa in the last 1000 years contrasts with the heterogeneity of the lithotypes revealed by the perforations. Moreover, partial melting of latitic and trachytic lithologies is inconsistent with the low content of Ba, Sr and the high Eu anomaly that, in turn, are better explained by processes of crystal fractionation plus a small amount of crustal assimilation (Fig. 12).

As alternative to partial melting of shallow crustal rocks, the crystal-poor rhyolite could be explained in the light of efficient crystal-melt separation processes. It is widely accepted that the architecture of magmatic system, also those belonging to arc settings, should be envisaged in a "mush-dominating" perspective, where the melts and exsolved fluids are distributed within a crystalline network, in vertically developed systems (Cashman et al. 2017; Edmonds et al. 2019; Sparks et al. 2019). In this scenario, crystal-poor melts with evolved composition can be generated by the extraction from crystal mushes of intermediate composition favoured by efficient crystal–melt separation processes. These models include (i) compaction-induced segregation of melt and subsequent extrusion of interstitial melt in response to deformation and settling of a crystalline framework (Bachmann and Bergantz 2004), (ii) segregation of evolved liquid induced by gravitational instability of the upper solidification front (Marsh 2002; Masotta et al. 2012b) and (iii) filter-press induced by volatile exsolution (Pistone et al. 2015). Thermo-mechanical modelling suggests that melt extraction is more efficient at high crystal content between 50 and 70% (Dufek and Bachmann 2010). In this context, volatile exsolution plays a fundamental role on the physical and rheological properties of melt produced within mush-dominated regions of such systems (Parmigiani et al. 2014; Edmonds et al. 2019). When the fluid exsolution is reached, in a system largely dominated by a high crystal fraction (50–70%), the volatile phase is concentrated in narrow channels (Oppenheimer et al. 2015) that may favour the segregation of melt locked in the crystal network through gas-driven filter pressing (Sisson et al. 1999; Pistone et al. 2015). A similar process was also observed in temperature gradient experiments by Rodriguez et al. (2017), who described the migration through the crystal mush of a fluid phase exsolved in it through second boiling (i.e. volatile exsolution induced by isobaric crystallization). At La Fossa volcano, pre-eruptive volatile exsolution is likely to occur at the rhyolite stage in the shallow system (Gioncada et al. 1998; Fulignati et al. 2018). Following these considerations, we suggest that rhyolitic magmas at La Fossa could be generated by AFC processes within crystal mushes, being eventually extracted favoured by the exsolved fluid phase. The effects of the fluid phase are twofold as they contribute to (i) rejuvenating the crystal mush through the increase of the melt fraction (Pistone et al. 2017) and (ii) decreasing the melt viscosity, in turn favouring the melt extraction from the crystal mush (Ardia et al. 2008; Pistone et al. 2013). These processes can be even more effective in the case of a mush system that approaches the second boiling upon late solidification (Edmonds et al. 2019). In this framework, the volcanic unrests occurred between AD 1977 and 1999 and in AD 2004 culminated, only in an intensification of the fumarolic temperatures and in changes of the chemical compositions of the gases discharged, were possibly caused by the second boiling of the intermediate mushy magmas, not followed by remobilization of the interstitial melt. Indeed, the changes in the fumarolic activity have not been accompanied by deep seismicity and ground deformation, suggesting that no movement of magma occurred at shallow levels (Granieri et al. 2006; Paonita et al. 2013).

If we assume that the latitic–trachytic magmas represent the closest parental compositions from which the rhyolitic magma originated, it is important to consider the genetic relationship between the rhyolite and the latitic–trachytic enclaves. In the similar context of Lipari Island, Davì et al. (2010) demonstrated that the rhyolitic magma feeding the Rocche Rosse lava flow was produced through AFC processes, starting from the latitic magma compositions represented by magmatic enclaves contained in the rhyolitic lava. These enclaves, according to Forni et al. (2015), represent remobilized and partially melted portions of the crystal mush from which the rhyolitic melt originated. In a similar fashion, the coexistence of latitic–trachytic and rhyolitic magmas in the eruptive products of La Fossa testifies to the presence of magmas belonging to the same liquid line of descent, but yielding to different types of interaction. The contrasting rheological behaviour of the crystal-rich latitic–trachytic enclaves and the host rhyolitic magma, as in the case of the Pietre Cotte obsidian, suggests that very different rheology characterized the two magma domains (i.e. the enclaves were entrained in a nearly solid state; P.I. = 25–30%). In contrast, in the case of mingled products of Pietre Cotte pumices and the Commenda lava, the trachytic–latitic domain had similar rheological behaviour. Consistently, the crystal content of the latitic–trachytic domain (P.I. ranging from 3 to 30%) overlaps only in part the crystallinity range that defines the

magma as a crystal mush (25–50%; Marsh 1996) and that in turn allows to classify the magmatic enclaves of Pietre Cotte as remobilized fragments of the crystal mush (Fig. 13).

The remobilization of the crystal mush could have been favoured by the arrival of a new batch of hotter (latitic) magma. Assuming that part of this magma was also erupted (e.g. evidence for the eruption of a latitic magma is the banding in the Pietre Cotte pumices and Commenda lava), the remaining part interacted with the crystal mush at depth. The melting of lower temperature phases such as alkali feldspar and biotite, almost absent in magmatic enclaves, but necessary to form rhyolitic magma (see Sect. 6.2), reduced the crystallinity and promoted the hydration and remobilization of the crystal mush. The previously extracted rhyolitic melt and the remobilized portions of the crystal mush (i.e. enclaves and glomerocrysts) are thus erupted together (Fig. 13). This is also evident in the geochemical characteristics of the magmatic enclaves of Pietre Cotte, where high-Sr plagioclase (Piochi et al. 2009) is often surrounded by an overgrowth of sanidine, related to the crystallization from a melt originated by partial melting of a feldspar-rich crystal mush (Forni et al. 2015). The overall texture of magmatic enclaves and, more in general, of the lati-trachytic magmas that exhibit a broad range of crystal size, shape and textures (including glomerocrysts; Fig. 3a, b) supports this hypothesis. This variability may be caused not only by the repeated episodes of mafic recharge, magma ascent and mixing in short time scales (1–10 years, Nicotra et al. 2018), but also by the variable degree of interaction of the mafic magmas with the crystal mushes.

Concluding remarks

The complex relationships among latitic, trachytic and rhyolitic magmas erupted at La Fossa volcano in the last 1000 years are unveiled by mineral–liquid thermo-barometry and hygrometry, geochemical modelling and temperature gradient experiments. By combining this information with the petrographic analysis of explosive and effusive products, a new model of the polybaric magmatic system is obtained and the following conclusions can be drawn:

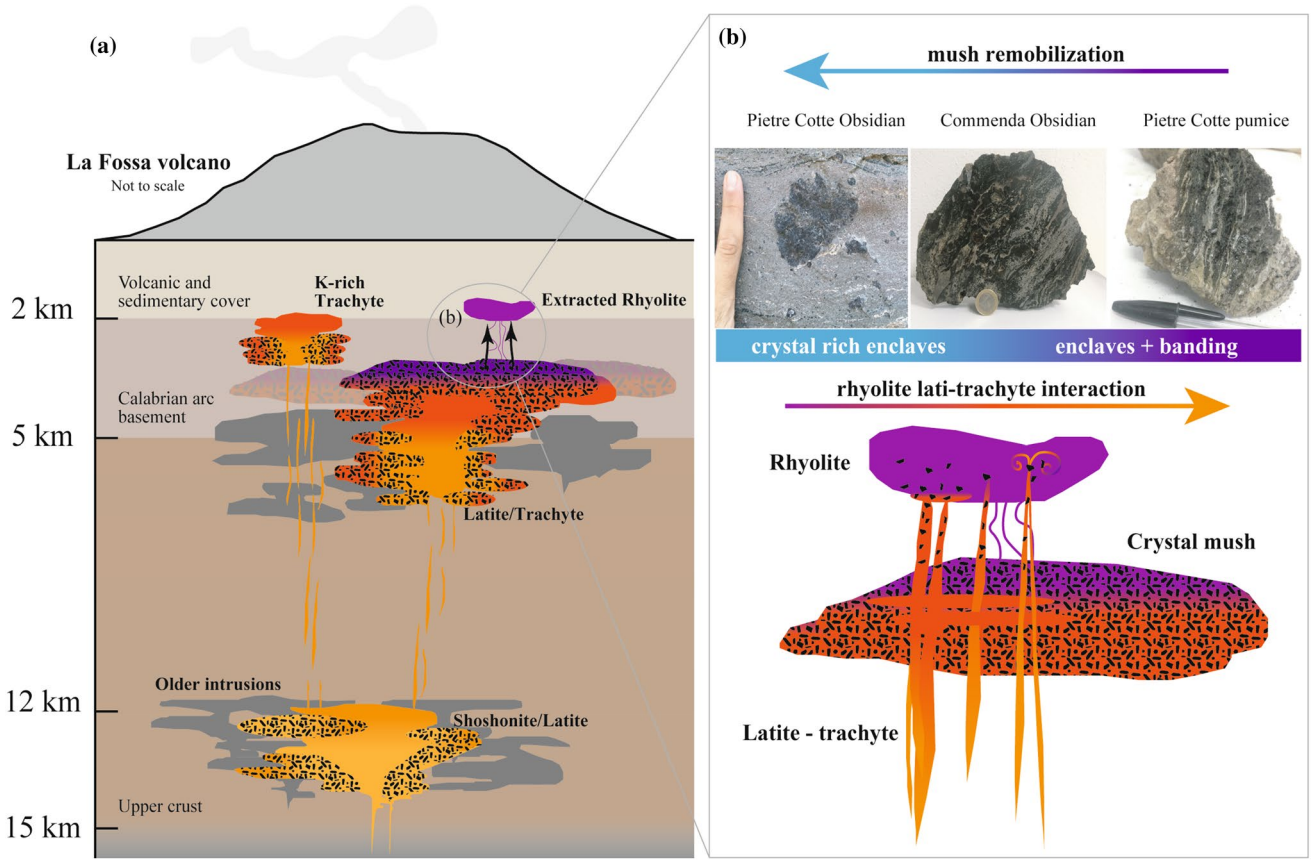

Fig. 13 **a** Sketch representation showing the depth of the reservoirs that have been active at La Fossa volcano in the last 1000 years (depths and crustal structure after Peccerillo et al. 2006) and **b** of the extraction of crystal-poor rhyolite from the crystal mush. The different interaction between the recharging magmas and the rhyolite explains the petrologic features of the recent eruptive products of La Fossa

- the latitic magma represents the least differentiated composition erupted at La Fossa volcano in the last 1000 years and the closest parental magma for both K-rich (Pal D) and normal trachytes (Palizzi lava flow);
- the K-rich trachytic magma of Pal D originated at lower depth (corresponding to 160 ± 54 MPa) and less hydrous conditions compared to normal trachytic magmas (208 ± 30 MPa);
- the rhyolitic melt originated within the latitic–trachytic crystal mush and eventually segregated into crystal-poor batches, upon increased volatile concentration in the fluid phase (i.e. second boiling of mushy magmas), through gas filter pressing process;
- latitic and trachytic enclaves and mingled bands in rhyolites, as well as glomerocrysts, testify to disrupted portions of the crystal mush (i.e. highly porphyritic enclaves) and the mafic (latitic) magma responsible for the mush remobilization.

Acknowledgements The authors thank the editor and the two anonymous reviewers for their valuable comments, A. Risplendente (Università di Milano), O. Bruguier (Université de Montpellier), R. Ishak (Università di Pisa), L. Ghezzi (Università di Pisa) for assistance during analytical work and F. Colarieti, M. Gemelli (Università di Pisa) for samples preparation. The research was funded by Università di Pisa "FFABR—Ricerca di Base" to AG, "FFABR—Ricerca di Base" and "PRA 2018—Progetti di Ricerca di Ateneo" to MM and MP and by the Italian Ministero dell'Istruzione, dell'Università e della Ricerca (MIUR) through the Progetti di Rilevante Interesse Nazionale (PRIN) "Time scales of solidification in magmas: Applications to Volcanic Eruptions, Silicate Melts, Glasses, Glass–Ceramics" project (PRIN2017J277S9) to MM. This research is part of SC PhD program funded by a Tuscany Regional "Pegaso" doctoral grant.

References

Ardia P, Giordano D, Schmidt MW (2008) A model for the viscosity of rhyolite as a function of H_2O-content and pressure: a calibration based on centrifuge piston cylinder experiments. Geochim Cosmochim Acta 72(24):6103–6123

Bachmann O, Bergantz GW (2004) On the origin of crystal-poor rhyolites: extracted from batholithic crystal mushes. J Petrol 45(8):1565–1582

Beermann O, Holtz F, Duesterhoeft E (2017) Magma storage conditions and differentiation of the mafic Lower Pollara volcanics, Salina Island, Aeolian Islands, Italy: implications for the formation conditions of shoshonites and potassic rocks. Contrib Miner Petrol 172(5):37

Biass S, Bonadonna C, Di Traglia F, Pistolesi M, Rosi M, Lestuzzi P (2016) Probabilistic evaluation of the physical impact of future tephra fallout events for the Island of Vulcano, Italy. Bull Volcanol 78(5):37

Brugman KK, Till CB (2019) A low-aluminum clinopyroxene-liquid geothermometer for high-silica magmatic systems. Am Miner 104(7):996–1004

Bullock LA, Gertisser R, O'Driscoll B, Harland S (2019) Magmatic evolution and textural development of the 1739 CE Pietre Cotte lava flow, Vulcano, Italy. J Volcanol Geoth Res 372:1–23

Cashman KV, Sparks RSJ, Blundy JD (2017) Vertically extensive and unstable magmatic systems: a unified view of igneous processes. Science 355(6331):eaag3055

Cioni R, Marianelli P, Santacroce R (1998) Thermal and compositional evolution of the shallow magma chambers of Vesuvius: evidence from pyroxene phenocrysts and melt inclusions. J Geophys Res Solid Earth 103(B8):18277–18294

Clocchiatti R, Del Moro A, Gioncada A, Joron JL, Mosbah M, Pinarelli L, Sbrana A (1994) Assessment of a shallow magmatic system: the 1888–90 eruption, Vulcano Island, Italy. Bull Volcanol 56(6–7):466–486

Davì M, De Rosa R, Donato P, Vetere F, Barca D, Cavallo A (2009) Magmatic Evolution and plumbing system of ring-fault volcanism: the Vulcanello Peninsula (Aeolian Islands, Italy). Eur J Mineral 21(5):1009–1028

Davì M, De Rosa R, Holtz F (2010) Mafic enclaves in the rhyolitic products of Lipari historical eruptions; relationships with the coeval Vulcano magmas (Aeolian Islands, Italy). Bull Volcanol 72(8):991–1008

De Astis G, La Volpe L, Peccerillo A, Civetta L (1997) Volcanological and petrological evolution of Vulcano Island (Aeolian Arc, southern Tyrrhenian Sea). J Geophys Res Solid Earth 102(B4):8021–8050

De Astis G, Lucchi F, Dellino P, La Volpe L, Tranne CA, Frezzotti ML, Peccerillo A (2013) Geology, volcanic history and petrology of Vulcano (central Aeolian archipelago). Geol Soc Lond Mem 37(1):281–349

De Fino M, La Volpe L, Piccarreta G (1991) Role of magma mixing during the recent activity of La Fossa di Vulcano (Aeolian Islands, Italy). J Volcanol Geoth Res 48(3–4):385–398

Del Moro A, Gioncada A, Pinarelli L, Sbrana A, Joron JL (1998) Sr, Nd, and Pb isotope evidence for open system evolution at Vulcano, Aeolian Arc, Italy. Lithos 43(2):81–106

Di Traglia F, Pistolesi M, Rosi M, Bonadonna C, Fusillo R, Roverato M (2013) Growth and erosion: the volcanic geology and morphological evolution of La Fossa (Island of Vulcano, Southern Italy) in the last 1000 years. Geomorphology 194:94–107

Dufek J, Bachmann O (2010) Quantum magmatism: Magmatic compositional gaps generated by melt-crystal dynamics. Geology 38(8):687–690

Edmonds M, Cashman KV, Holness M, Jackson M (2019) Architecture and dynamics of magma reservoirs. Architecture and dynamics of magma reservoirs. Philos Trans R Soc A 377:2139. https://doi.org/10.1098/rsta.2018.0298

Faraone D, Silvano A, Verdiani G (1986) The monzogabbroic intrusion in the island of Vulcano, Aeolian Archipelago, Italy. Bull Volcanol 48(5):299–307

Forni F, Ellis BS, Bachmann O, Lucchi F, Tranne CA, Agostini S, Dallai L (2015) Erupted cumulate fragments in rhyolites from Lipari (Aeolian Islands). Contrib Miner Petrol 170(5–6):49

Frazzetta G, La Volpe L, Sheridan MF (1983) Evolution of the Fossa cone, Vulcano. J Volcanol Geoth Res 17(1–4):329–360

Frezzotti ML, Peccerillo A, Zanon V, Nikogosian I (2004) Silica-rich melts in quartz xenoliths from Vulcano Island and their bearing on processes of crustal anatexis and crust–magma interaction beneath the Aeolian Arc, Southern Italy. J Petrol 45(1):3–26

Fusillo R, Di Traglia F, Gioncada A, Pistolesi M, Wallace PJ, Rosi M (2015) Deciphering post-caldera volcanism: insight into the Vulcanello (Island of Vulcano, Southern Italy) eruptive activity based on geological and petrological constraints. Bull Volcanol 77(9):76

Fulignati P, Gioncada A, Costa S, Di Genova D, Di Traglia F, Pistolesi M (2018) Magmatic sulfide immiscibility at an active magmatic-hydrothermal system: The case of La Fossa (Vulcano, Italy). J Volcanol Geoth Res 358:45–57

Gioncada A, Clocchiatti R, Sbrana A, Bottazzi P, Massare D, Ottolini L (1998) A study of melt inclusions at Vulcano (Aeolian

Islands, Italy): insights on the primitive magmas and on the volcanic feeding system. Bull Volcanol 60(4):286–306
Gioncada A, Sbrana A (1991) "La Fossa caldera", Vulcano: inferences from deep drillings. Acta Vulcanol 1:115–126
Granieri D, Carapezza ML, Chiodini G, Avino R, Caliro S, Ranaldi M, Tarchini L (2006) Correlated increase in CO_2 fumarolic content and diffuse emission from La Fossa crater (Vulcano, Italy): evidence of volcanic unrest or increasing gas release from a stationary deep magma body? Geophys Res Lett 33(13):L13316. https://doi.org/10.1029/2006GL026460
Gurioli L, Zanella E, Gioncada A, Sbrana A (2012) The historic magmatic-hydrothermal eruption of the Breccia di Commenda, Vulcano, Italy. Bull Volcanol 74(5):1235–1254
Huang F, Lundstrom CC, Glessner J, Ianno A, Boudreau A, Li J, Ferréc EC, Marshaka S, DeFrates J (2009) Chemical and isotopic fractionation of wet andesite in a temperature gradient: experiments and models suggesting a new mechanism of magma differentiation. Geochim Cosmochim Acta 73(3):729–749
Keller J (1980) The island of Vulcano. Rendiconti della società Italiana di Mineralogia e Petrologia 36:368–413
Laumonier M, Laporte D, Faure F, Provost A, Schiano P, Ito K (2019) An experimental study of dissolution and precipitation of forsterite in a thermal gradient: implications for cellular growth of olivine phenocrysts in basalt and melt inclusion formation. Contrib Miner Petrol 174(11):94
Mandarano M, Paonita A, Martelli M, Viccaro M, Nicotra E, Millar IL (2016) Revealing magma degassing below closed-conduit active volcanoes: geochemical features of volcanic rocks versus fumarolic fluids at Vulcano (Aeolian Islands, Italy). Lithos 248:272–287
Marsh BD (1996) Solidification fronts and magmatic evolution. Miner Mag 60(398):5–40
Marsh BD (2002) On bimodal differentiation by solidification front instability in basaltic magmas, part 1: basic mechanics. Geochim Cosmochim Acta 66(12):2211–2229
Masotta M, Freda C, Paul TA, Moore GM, Gaeta M, Scarlato P, Troll VR (2012a) Low pressure experiments in piston cylinder apparatus: calibration of newly designed 25 mm furnace assemblies to P= 150 MPa. Chem Geol 312:74–79
Masotta M, Freda C, Gaeta M (2012b) Origin of crystal-poor, differentiated magmas: insights from thermal gradient experiments. Contrib Miner Petrol 163(1):49–65
Masotta M, Mollo S, Freda C, Gaeta M, Moore G (2013) Clinopyroxene–liquid thermometers and barometers specific to alkaline differentiated magmas. Contrib Miner Petrol 166(6):1545–1561
Masotta M, Mollo S, Nazzari M, Tecchiato V, Scarlato P, Papale P, Bachmann O (2018) Crystallization and partial melting of rhyolite and felsite rocks at Krafla volcano: a comparative approach based on mineral and glass chemistry of natural and experimental products. Chem Geol 483:603–618
Masotta M, Mollo S (2019) A new plagioclase-liquid hygrometer specific to trachytic systems. Minerals 9(6):375
Masotta M, Pontesilli A, Mollo S, Armienti P, Ubide T, Nazzari M, Scarlato P (2020) The role of undercooling during clinopyroxene growth in trachybasaltic magmas: Insights on magma decompression and cooling at Mt. Etna Volcano Geochimica et Cosmochimica Acta 268:258–276
Mollo S, Masotta M (2014) Optimizing pre-eruptive temperature estimates in thermally and chemically zoned magma chambers. Chem Geol 368:97–103
Mollo S, Putirka K, Misiti V, Soligo M, Scarlato P (2013) A new test for equilibrium based on clinopyroxene-melt pairs: clues on the solidification temperatures of Etnean alkaline melts at post-eruptive conditions. Chem Geol 352:92–100
Mollo S, Masotta M, Forni F, Bachmann O, De Astis G, Moore G, Scarlato P (2015) A K-feldspar–liquid hygrometer specific to alkaline differentiated magmas. Chem Geol 392:1–8
Neri A, Aspinall WP, Cioni R, Bertagnini A, Baxter PJ, Zuccaro G, Hincks TK (2008) Developing an event tree for probabilistic hazard and risk assessment at Vesuvius. J Volcanol Geoth Res 178(3):397–415
Nicotra E, Giuffrida M, Viccaro M, Donato P, D'Oriano C, Paonita A, De Rosa R (2018) Timescales of pre-eruptive magmatic processes at Vulcano (Aeolian Islands, Italy) during the last 1000 years. Lithos 316:347–365
Oppenheimer J, Rust AC, Cashman KV, Sandnes B (2015) Gas migration regimes and outgassing in particle-rich suspensions. Front Phys 3:60
Paonita A, Federico C, Bonfanti P, Capasso G, Inguaggiato S, Italiano F, Sortino F (2013) The episodic and abrupt geochemical changes at La Fossa fumaroles (Vulcano Island, Italy) and related constraints on the dynamics, structure, and compositions of the magmatic system. Geochim Cosmochim Acta 120:158–178
Parmigiani A, Huber C, Bachmann O (2014) Mush microphysics and the reactivation of crystal-rich magma reservoirs. J Geophys Res Solid Earth 119(8):6308–6322
Peccerillo A, Frezzotti ML, De Astis G, Ventura G (2006) Modeling the magma plumbing system of Vulcano (Aeolian Islands, Italy) by integrated fluid-inclusion geobarometry, petrology, and geophysics. Geology 34(1):17–20
Perinelli C, Mollo S, Gaeta M, De Cristofaro SP, Palladino DM, Armienti P, Putirka KD (2016) An improved clinopyroxene-based hygrometer for Etnean magmas and implications for eruption triggering mechanisms. Am Miner 101(12):2774–2777
Perugini D, Valentini L, Poli G (2007) Insights into magma chamber processes from the analysis of size distribution of enclaves in lava flows: a case study from Vulcano Island (Southern Italy). J Volcanol Geoth Res 166(3–4):193–203
Pinarelli L, Gioncada A, Capaccioni B, Vaselli O, Downes H (2019) Mantle source heterogeneity in subduction zones: constraints from elemental and isotope (Sr, Nd, and Pb) data on Vulcano Island, Aeolian Archipelago, Italy. Mineral Petrol 113(1):39–60
Piochi M, De Astis G, Petrelli M, Ventura G, Sulpizio R, Zanetti A (2009) Constraining the recent plumbing system of Vulcano (Aeolian Arc, Italy) by textural, petrological, and fractal analysis: the 1739 AD Pietre Cotte lava flow. Geochem Geophys Geosyst 10(1):Q01009. https://doi.org/10.1029/2008GC002176
Pistone M, Arzilli F, Dobson KJ, Cordonnier B, Reusser E, Ulmer P, Blundy JD (2015) Gas-driven filter pressing in magmas: Insights into in-situ melt segregation from crystal mushes. Geology 43(8):699–702
Pistone M, Blundy J, Brooker RA (2017) Water transfer during magma mixing events: Insights into crystal mush rejuvenation and melt extraction processes. Am Miner 102(4):766–776
Pistone M, Caricchi L, Ulmer P, Reusser E, Ardia P (2013) Rheology of volatile-bearing crystal mushes: mobilization vs. viscous death. Chem Geol 345:16–39
Pontesilli A, Masotta M, Nazzari M, Mollo S, Armienti P, Scarlato P, Brenna M (2019) Crystallization kinetics of clinopyroxene and titanomagnetite growing from a trachybasaltic melt: New insights from isothermal time-series experiments. Chem Geol 510:113–129
Putirka KD (2008) Thermometers and barometers for volcanic systems. Rev Mineral Geochem 69(1):61–120
Rodríguez C, Castro A (2017) Silicic magma differentiation in ascent conduits. Experimental constraints. Lithos 272:261–277
Rodríguez C, Geyer A, Castro A, Villaseñor A (2015) Natural equivalents of thermal gradient experiments. J Volcanol Geoth Res 298:47–58

Rosi M, Di Traglia F, Pistolesi M, Ongaro TE, Vitturi MDM, Bonadonna C (2018) Dynamics of shallow hydrothermal eruptions: new insights from Vulcano's Breccia di Commenda eruption. Bull Volcanol 80(12):83

Rossi S, Petrelli M, Morgavi D, Vetere F, Almeev RR, Astbury RL, Perugini D (2019) Role of magma mixing in the pre-eruptive dynamics of the Aeolian Islands volcanoes (Southern Tyrrhenian Sea, Italy). Lithos 324:165–179

Scaillet B, Pichavant M, Cioni R (2008) Upward migration of Vesuvius magma chamber over the past 20,000 years. Nature 455(7210):216

Shea T, Hammer JE (2013) Kinetics of cooling-and decompression-induced crystallization in hydrous mafic-intermediate magmas. J Volcanol Geoth Res 260:127–145

Sisson TW, Bacon CR (1999) Gas-driven filter pressing in magmas. Geology 27(7):613–616

Sparks RSJ, Annen C, Blundy JD, Cashman KV, Rust AC, Jackson MD (2019) Formation and dynamics of magma reservoirs. Philos Trans R Soc A 377(2139):20180019

Sun C, Liang Y (2017) A REE-in-plagioclase–clinopyroxene thermometer for crustal rocks. Contrib Miner Petrol 172(4):24

Vetere F, Petrelli M, Morgavi D, Perugini D (2015) Dynamics and time evolution of a shallow plumbing system: the 1739 and 1888–90 eruptions, Vulcano Island, Italy. J Volcanol Geoth Res 306:74–82

Zanon V, Frezzotti ML, Peccerillo A (2003) Magmatic feeding system and crustal magma accumulation beneath Vulcano Island (Italy): evidence from CO_2 fluid inclusions in quartz xenoliths. J Geophys Res Solid Earth. https://doi.org/10.1029/2002JB002140